Thermal Storage for Electric Vehicle Cabin Heating in Cold Weather Conditions

THERMAL STORAGE FOR ELECTRIC VEHICLE CABIN HEATING IN COLD WEATHER CONDITIONS

BY

TREVOR HADDEN, B. Eng.

A THESIS

SUBMITTED TO THE DEPARTMENT OF MECHANICAL ENGINEERING

AND THE SCHOOL OF GRADUATE STUDIES

OF MCMASTER UNIVERSITY

IN PARTIAL FULFILMENT OF THE REQUIREMENTS

FOR THE DEGREE OF

MASTER OF APPLIED SCIENCE

Master of Applied Science (2017) McMaster University

(Mechanical Engineering) Hamilton, Ontario, Canada

TITLE:	Thermal Storage for Electric Vehicle Cabin Heating in Cold Weather Conditions
AUTHOR:	Trevor Hadden Bachelor of Engineering, Sustainable and Renewable Energy: Stream B Carleton University, Ottawa ON, Canada
SUPERVISOR:	Dr. Ali Emadi and Dr. James Cotton
NUMBER OF PAGES:	xviii,119

I would like to dedicate this thesis to my parents.

Abstract

With global warming, an inevitable threat to humanity, significant efforts in all carbon emitting industries are required. Electric vehicles are a suitable alternative to the petroleum dominated automotive industry. However, obstacles like charging infrastructure and limited range still stand in the way of their continued acceptance. This limited driving range can be further reduced in cold weather due to decreased battery efficiency and increased heating load. The heating in most electric vehicles is provided by an electrical positive temperature coefficient resistor. This architecture can lead to reductions in range of over 50 %.

A thermal storage system has been devised and presented in this thesis which can partially or fully offset the thermal requirements. This is accomplished by pre-heating a thermal storage tank which then uses sensible energy to provide the heat for the cabin and battery pack. The system has been shown to reduce consumption and improve driving range in low ambient temperature conditions. This system successfully offers a potential solution to the concern of large range fluctuations due to different ambient temperatures.

After producing a representative electric vehicle model in AMESim, it was compared to the Nissan Leaf with acceptable errors. The range implications for this baseline electric vehicle are then presented. A coolant based, thermal storage tank is

then added to the model and simulated across a variety of temperatures and thermal storage masses. The results show that a 80 kg, 80 °C coolant tank can provide all the heating requirements for a 36 km, one hour and 9 minute city drive cycle. Offering a calculated consumption reduction of up to 36 % at -30 °C as compared to the baseline electric vehicle model. Furthermore, a yearly analysis was performed based on this cycle and the results have shown that an optimal 30 kg thermal storage tank can decrease the yearly average consumption by up to 20 Wh/km or 12 %.

Acknowledgements

This research was undertaken, in part, thanks to funding from the Canada Excellence Research Chairs Program. The research would not have been made possible without the simulation software AMESim. I would like thank Dr. Ali Emadi and everyone at MARC as well as Dr. James Cotton and the entire TMRL group at McMaster.

List of abbreviations

BEV	Battery Electric Vehicle
CS	Cold start
EV	Electric Vehicle
HS	Hot Start
HEV	Hybrid Electric Vehicle
ICE	Internal Combustion Engine
UDDS	Urban Dynamometer Driving Schedule
HWFET	Highway Fuel Economy Test
HWY	Highway
PCM	Phase Change Material
PHEV	Plug-in Hybrid Electric Vehicle
PTC	Positive Temperature Coefficient
SoC	State-of-Charge
TES	Thermal Energy Storage
TS	Thermal Storage

Contents

List of Figures

Chapter 1

Introduction and Problem Statement

1.1 Introduction

Global warming is a reality which threatens the quality of life on planet earth. The earth's surface and atmosphere are being warmed at an alarming rate which is likely caused by the emission of greenhouse gases such as carbon dioxide. Carbon dioxide is the product of all fossil fuel combustion which gets trapped in the atmosphere for up to two thousand years, blocking infrared radiation leaving the earth's surface thus causing a warming effect [1], [2]. Several gases and economic sectors contribute to the warming of the earth and a break-down of the global emissions can be seen in Fig. 1.1. The largest contributer in carbon dioxide, coming primarily from industry, electricity and heat generation, agriculture and transportation. UN policy makers around the world are coming together to set carbon emission reduction targets due to evidence

of global warming provided by the International Panel of Climate Change [2]. In Ontario, Canada, the provincial government has set a goal of 15 % reduction by 2020, 37 % by 2030 and 80 % by 2050 [3]. This will be done with the use of various policies limiting the carbon emissions for each sector. These policies are present in, and will continue to extend into the transportation industry thus creating a need for alternatively fuelled vehicles. Roughly 95 % of the worlds vehicles run on petroleum-based fuels [4], and in Ontario a third of emissions are from this sector [3]. Electrification

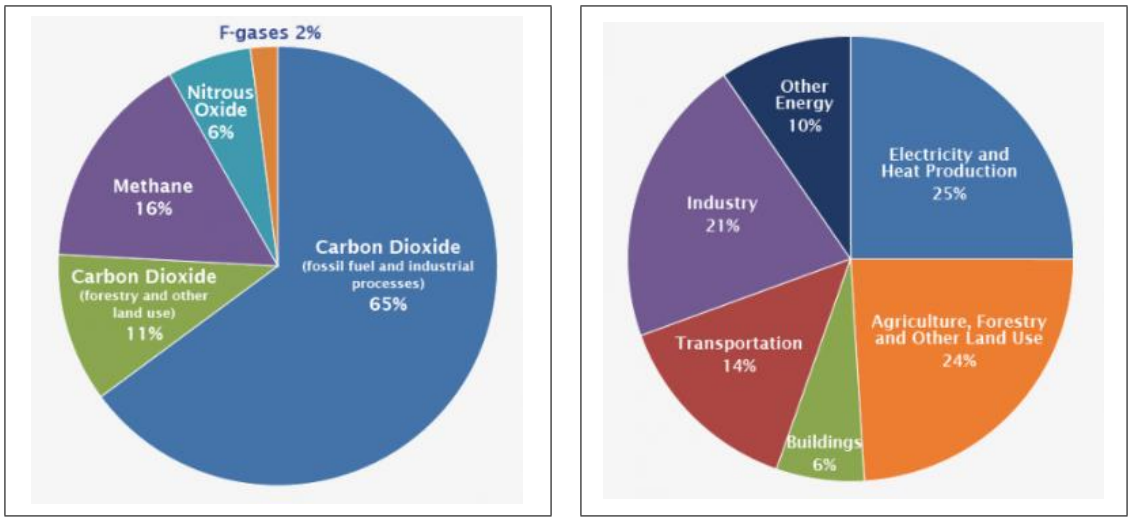

(a) By gas. (b) By economic sector.

Figure 1.1: Global Emissions [4].

is considered as the best option for the reduction of emissions in most industries, provided the electricity generation sector can meet emission requirements with an increased demand. In the transportation industry, the electrification process is already well underway. Many challenges still face the electrification process including lack of range and charging infrastructure for electric vehicles. Additionally, the range of electric vehicles suffers further in cold weather due to increased heating requirements and decreased battery efficiency. Drivers in mild ambient conditions could have their

ranges reduced more than 50 % when driving sub-freezing temperatures [5]. In places with both extreme cold temperatures as well as mild temperatures, the variation in range throughout the year can be significant. Adding more batteries would extend the range in both seasons, however this would not address the inconsistency of the vehicle range. New heating strategies must be explored in order reduce the range reduction in cold climates. Accomplishing this task would increase the feasibility of electric vehicles and therefore allowing further attenuation of carbon emissions.

The electric vehicle heating system explored in this research employs a thermal storage tank which when preheated could offset some or all of the vehicle heat requirements. Upon charging the electric battery the thermal storage would also be charged (heated). Once disconnected from the grid, the cabin and battery heat would be initially provided by the thermal storage tank. The storage material was selected to be an ethylene-glycol/water mixture to ensure easy incorporation into most systems. The significance of the consumption reduction and therefore the range savings is dependent upon the duration and type of the drive, the size of the tank and its initial temperature, and the outside temperature. It has been shown that an 80 kg, 80 °C storage tank could decrease the consumption by up to 36 % for a 1 hour and 9 minute, city drive cycle in -30 °C climate. Additionally, it has been shown that a 30 kg TS tank could decrease the yearly average consumption by up to 20 Wh/km.

This thesis is comprised of several chapters, starting with Chapter 2 where the impact of vehicle heating on driving range is discussed as well as a review vehicle heating methods. In Chapter 3, the simulation software and the details of the EV model are introduced. The simulation results are then compared to Nissan Leaf dynamometer data from [6]. Once the model was sufficiently accurate, it was simulated through a

variety of ambient temperatures and driving profiles. These results can be found in Chapter 4. With a baseline established, the thermal storage system is conceptually explained in Chapter 5 and the model modifications are presented along with heat loss calculations and the effect of mass addition on range. Chapter 6 presents the results of this new vehicle model possessing thermal storage. In Chapter 7, some short comings of the vehicle's HVAC controller are addressed, the charging implications are discussed and the yearly implications of the system are examined. Finally, Chapter 8, summarizes the research and provides some considerations for future work in this area.

Chapter 2

Energy Consumption for Electric Vehicle Heating and its Impact on Range

This chapter will provide some background information on the various topics related to the challenge of cold weather driving.

2.1 Description of Challenge

In many places of the world, including Canada, winters can be extremely cold. Double digit negative temperatures are normal and temperatures like -30° Celsius are not uncommon. A region with such a cold climate, certainly qualifies as one where heating systems are necessary. This poses an interesting challenge for battery electric vehicles (BEVs) which do not have an inefficient combustion process propelling the vehicle on board. BEVs must find other sources to obtain heat and keep passengers comfortable. Presently a common source of heat for BEVs is found by converting battery energy to electrical resistive heating. Such a design would have an impact

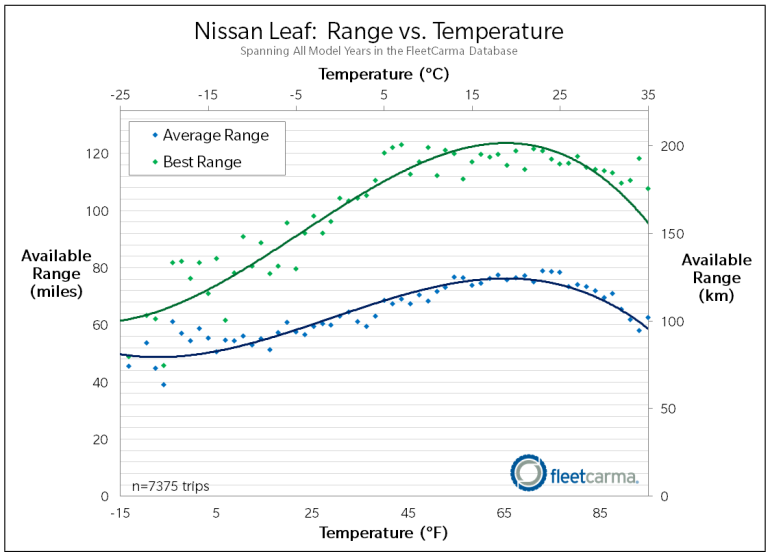

Figure 2.1: Range of the Nissan Leaf vs. temperature [7].

on vehicle range considering that the energy used for heating is the same as what is used for the vehicle propulsion system. Several studies have shown the range impact of cabin heating. In [7], information on over 7000 trips with the Nissan Leaf was recorded. Some of the results are plotted in Fig. 2.1 and Fig. 2.2 which display the

available range and the auxiliary power loads respectively as functions of ambient temperature. It is clear from Fig. 2.1 that the maximum range occurs around 18°

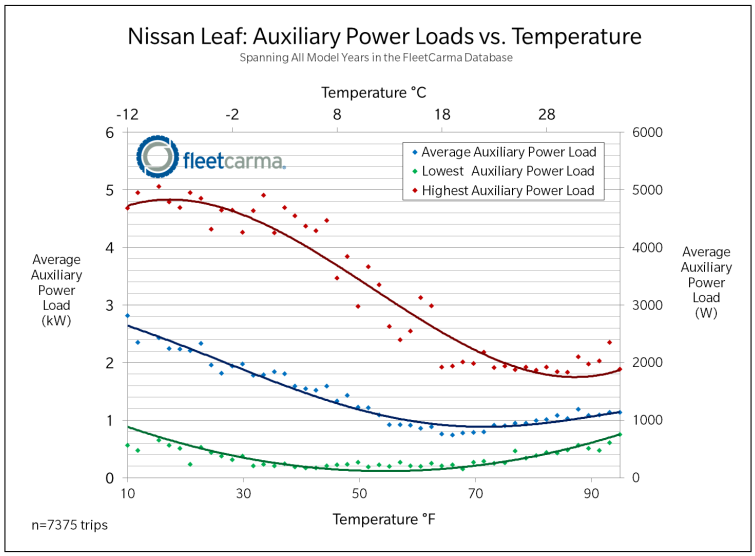

Figure 2.2: Auxiliary power consumption of the Nissan Leaf vs. temperature [7].

Celsius. This is the temperature where very little or no heating, ventilation or air conditioning (HVAC) is required. This is about the temperature where humans are most comfortable [8], [9]. At higher temperatures, air conditioning is required and at lower temperatures, heating is required. This thesis has only considered the implications of low temperatures on vehicle range and has omitted the discussion of range reduction due to air conditioning loads at high temperatures. The impact of range reduction due to air conditioning loads is less than the heating loads mainly due to the lower temperature difference compared to the reference 20° Celsius comfort temperature.

Since measuring the heater load directly can be difficult, the auxiliary power in [7], is considered to include the cabin heater, fan, battery heater, headlights, power steering, radio, USB charger, etc. Assuming all loads, other than those used for heating are constant with temperature, it becomes clear from these figures that low

ambient temperatures negatively impact the amount of energy required to heat BEVs, which in turn reduces the range. Further evidence of this phenomena can be seen in Fig. 2.3 where range reduced by almost 50 percent during a UDDS cycle. Other proof of this challenge can be seen in [5], [10] and [11] with some experimental results presented in [12].

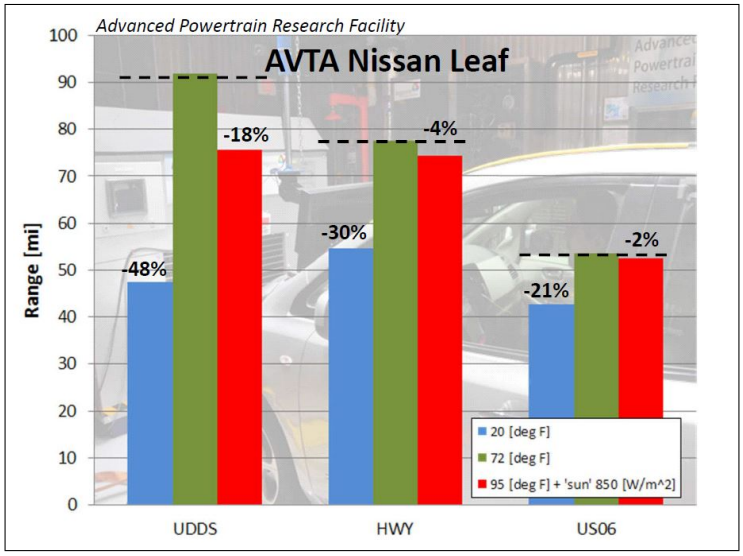

Figure 2.3: Range impact of temperature on the Nissan Leaf [6].

The impacts of temperature change on range for various drive cycles are illustrated in Fig. 2.3, showing that the most critical losses occur during a city cycle. The impact can still be observed in more aggressive, faster drive cycles such as the HWY cycle and the US06 cycle, but to a lesser extent. Thermal comfort in vehicles requires a lot of energy when the difference in ambient to desired temperature is large. The following section will examine the current methods used to heat automobiles.

2.2 Vehicle HVAC in Cold Weather

In order to address thermal comfort in vehicles, car manufacturers have developed several different solutions. These solutions are aimed at keeping the cabin at an adequate temperature and ensuring defogging and de-icing capabilities. HVAC issues are present in all types of vehicles including internal combustion engine, hybrid-electric and battery electric vehicles. The following section will outline several prominent HVAC systems which have been and/or are currently installed in ICEs, HEVs or EVs. Additionally, some upcoming technologies for EV heating will be discussed.

2.2.1 ICE cabin Heating

In a standard fossil fuel combustion vehicle, it is well known that around 30 percent of the energy in the fuel burned is converted to mechanical energy, that leaves significant waste heat which is either exhausted out of the tail pipe or moved to the radiator by coolant tubes where it is then dumped to the atmosphere. Alternatively, the heat can be directed to the cabin for heating. Similar to cogeneration plants, the waste heat is put to use heating the cabin, without the need to burn any additional fuel. In Fig. 2.4, a typical heating system is outlined by the red components. Coolant is pumped around the engine block by means of a mechanical or electrical pump, collecting waste heat which is then sent through a heat exchanger, called a heater core. Air is heated as it passes through the heater core and is distributed to the cabin air vents. This process keeps the engine temperature down and heats the cabin up which is ideal in low temperature environments. However in scenarios where the cabin does not require heat (warm ambient conditions), the coolant is diverted to a radiator in the front of the vehicle in order to dissipate heat to the environment and

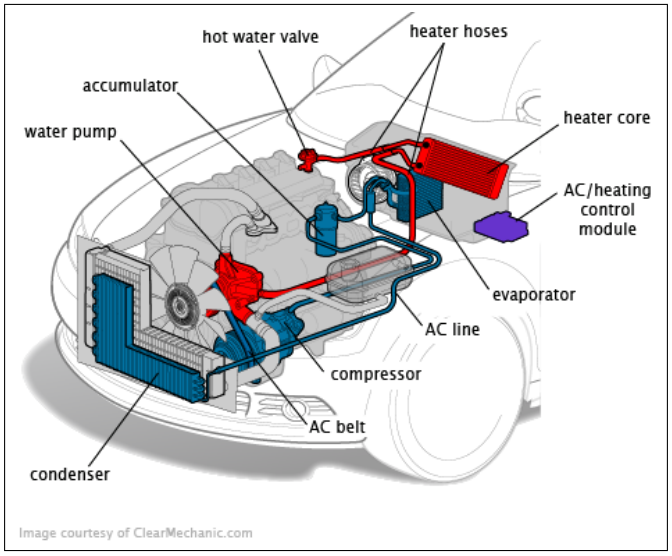

Figure 2.4: Standard ICE heating and cooling system [13].

prevent over-heating. This type of vehicle architecture provides more than enough heat for cold weather conditions and is the status quo. However, some ICE vehicles and mild hybrids have become so efficient that additional auxiliary electrical heaters are installed to assist with vehicle heating in extremely cold conditions [14]. Mild hybrid vehicles also comprise a combustion engine and can make use of the same waste heat as in ICEs to provide thermal comfort to passengers.

Battery-electric vehicles (BEVs) and plug-in hybrid-electric vehicles (PHEVs) however, require different heating schemes and sources in order to heat their vehicle cabin since all powertrain components in electric powertrains operate at very high efficiencies and thus have little waste heat for cabin heating. PHEVs have a particularly interesting situation since they possess both an electrical based heater as well as a combustion engine on-board. Depending on the driving mode and planned trip, the heating is supplied differently to maximize range. More on control strategies of PHEVs considering HVAC loads can be found in [15]. This thesis research focuses

on BEVs, where the only available source of energy is in the electrical storage. There are several different techniques for electrical heating which will be outlined in the following section.

2.2.2 Electric Vehicle Cabin Heating

The most popular solution to heating EVs is resistive heating using a positive temperature coefficient (PTC) heater. This is the most simple solution for EV battery and cabin heating [16]. A PTC heater is an electrical resistor which increases in resistance as its temperature increases, thus protecting itself from overheating [17]. More information on types of PTC heaters and their operation can be found in [14], [18] and [19]. The primary concern with the PTC heater is that it uses significant battery energy to heat the vehicle which leads to range losses of over 50 % in extreme cold conditions as previously described.

Several methods have been proposed as alternatives for EV cabin heating. Among them are the less popular thermoelectric modules which have been outcast due to their poor efficiencies [16]. Fossil fuel heaters have also been suggested due the high energy density of the fuel [16]. However, these heaters produce harmful emissions which directly contradicts the very purpose of EVs. Another solution involves radiating panels which are used to warm the passenger through radiation at a reduced energy cost [20]. Zonal heating was discussed in [11], where the vehicle vents are extended and altered to make the drive feel warmer without warming the entire cabin. Also in [11], the impact of heated seats and steering wheel is discussed. This can make the driver feel warmer through conductive heat transfer which is typically more efficient than convection as the entire cabin does not have to be heated. Preconditioning,

while not a direct alternative to cabin heating, is another strategy which can be used to extend range by ensuring the vehicle is at a desired temperature, before departure, using grid energy. In [21], it is suggested that preconditioning can extend driving range up to 19 %. The most competitive technology seems to be the heat pump. Operating the AC heat pump in reverse to produce heat for the vehicle at a higher coefficient of performance (COP) than a PTC heater, thus heating the vehicle with a reduced energy consumption. The major concern with heat pumps is that in sub freezing temperatures, they begin to lose their efficiency and heating capabilities. Additionally, they require a defrost cycle that further reduces their effectiveness. Some heat pump system architectures and performances are presented in [10]. An in-depth review of current heat pump technologies can be seen in [16]. Other HVAC consideration include windshield defrosting and defogging. Every vehicle must be able to melt ice (defrosting) and remove condensation (defogging) from the front windshield by either heating it or dehumidifying the inside air [22], among which, the major concern, in cold conditions, is the defrosting capabilities. Another possible solution to electric vehicle cabin heating is with thermal storage.

2.2.3 Energy Storage

Various types of energy storage systems exist which have useful applications in EVs. In this section, a comparison of energy storage methods and their respective energy densities, power densities and costs are discussed. In electric vehicles, batteries are the most widely used [23]. More specifically, lithium ion (Li-ion) batteries are the most commonly used in the automotive industry however many other chemistries exist. Another electrical storage medium is the ultra-capacitor (UC). Some battery

and hybrid ultra-capacitor properties are presented in Table 2.1. From this table, it is observed that while batteries offer good energy densities, they lack in power density. Conversely, UCs have superior power densities but poor energy densities. The hybridization of these two energy sources can offer the power density of the UC with the energy density of the batteries and this technique is discussed in [23], [24] and [25]. Li-ion batteries were selected as the baseline to compare against various thermal storage options. Though progress has been, and continues to be made in the reduction of battery prices, they are still very high and constitute as one of the primary costs of manufacturing electric vehicles.

Table 2.1: Battery and ultra capacitor properties and costs from [25].

	Lead Acid	NiMH	Li-ion	Hybrid UC
Specific energy (Wh/kg)	30-50	60-120	100-265	2.84-120
Energy density (Wh/L)	50-80	140-300	250-730	5.6-140
Specific power (W/kg)	75-300	250-1000	250-340	2300-14,000
Power density (W/L)	10-400	80-300	100-210	2500-27,000
Power capacity Cost ($/kW)	175-600	150-1500	175-4000	50-320
Energy capacity Cost ($/ kWh)	150-400	150-1500	500-2500	600-50,000

There are two ways of storing thermal energy: sensible heat storage and latent heat storage. Sensible energy storage depends on three parameters which are the material mass (m), material specific heat (Cp) and the change in temperature of the material (ΔT). Each of these are directly proportional to the storage energy in a medium. All materials regardless of their phase can store energy as sensible heat. Some materials, such as water, have high specific heats and thus can hold more energy

per unit mass and unit of temperature difference. Selecting a material with a high specific heat is critical to improving storage energy density. Storing sensible heat is limited only by the freezing point and boiling point of the material where further changes to the temperature would cause a change of phase. Latent heat energy is absorbed or released by a material undergoing a constant temperature phase change. The phase change temperature and amount of energy released per kg will differ based on the material. A review of available thermal storage materials and their properties, for both sensible and latent heat storage, can be found in [26]. Generally speaking, electric batteries have far better energy densities but cost significantly more. The range reduction in cold weather could be overcome by adding more batteries which are to be used strictly for HVAC. Due to high costs of the batteries, a thermal storage solution was investigated. For simplicity and since this is a proof of concept research project, a coolant based thermal storage tank was used. Since the coolant temperature fluctuation was expected to be about as much as 50 °C, and the power draw as much as 6kW, phase change material (PCM) was not investigated, not to mention the increased complexity of such a system. However in [27], some vehicle applications of PCM are discussed. Instead, a TS system was inserted in-line with the existing vehicle coolant loop. A 50/50 ethylene-glycol/water mixture material was assumed with an average specific heat of 3.3 kJ/kg K.

The proposal of this research is to use a preheated thermal storage mass to provide the necessary heat for the vehicle. A similar solution was attempted and discussed in a review article of EV HVAC techniques [28], where a heat pump system with PCM thermal storage was explained as a potential EV heating system. The Tohoku Electric Myld system included a heat pump that used the PCM thermal storage as the

heat source for the heat pump. For air conditioning, the heat pump would operate in reverse. The author of the review paper [28], concluded that due to its energy density, the system could be replaced by additional batteries and have the range extended in both warm and cold conditions. However, this would simply improve the range of the vehicle without dealing with the larger fluctuation from summer to winter. In another article, range extension of up to 20 % is quoted for a similar PCM based thermal storage system [29]. A PCM storage was built and tested in this reference and based on the energy in the PCM, the range savings were extrapolated. However, drive cycle results were not provided in either article which is the principal contribution of this thesis.

Chapter 3

Electric Vehicle Modeling and Simulations using AMESim

This chapter will discuss the software used for the modelling as well as define the architecture and some of the parameters that were used in the reference EV model. Additionally, the model is compared and validated against the Nissan Leaf.

3.1 Electric Vehicle Modeling with AMESim

Electric vehicles are very complex systems which interlink several different types of subsystems. AMESim is a system level, cross disciplinary modelling software which allows for an entire system to be developed at once. It possesses several libraries including Thermal, Electrical, Mechanical, etc. which contain experimentally tested analytical blocks. AMESim was selected as the software for this research project due to its user-friendliness and vast libraries of predefined components. Additionally, the software comes with several pre-built systems including an one of an EV model. The research presented in this thesis pertains primarily to modifications to the HVAC systems and so a general electric vehicle model sufficed. The pre-built model used is shown in [30], where the AMESim EV model is broken down in order to show individual system performances and characteristics. Additionally, [30] uses a SFTP-US06 drive cycle to show the impacts of HVAC systems on vehicle range using the default EV model. This model is a demo model in AMESim and is entitled "`ElectricVehicle_with_AC.ame`". Since this research is focused on cold weather HVAC needs, the first modification to the model was to remove the air conditioning system. Other changes included moving the PTC heater from the low-voltage network to the high-voltage network, adding various power and energy sensors, and building a new heating system. The modified AMESim model used for the baseline simulations is illustrated in Fig. 3.1. The input to the model is a drive cycle which is simply a speed profile as a function of time, along with several initial conditions. Several drive cycles were analyzed during this research, though only results from the UDDS (city) and HWFET (highway) are discussed. In the model, the electrical components are in purple, the controls are in red, the coolant loop is in blue/orange, the

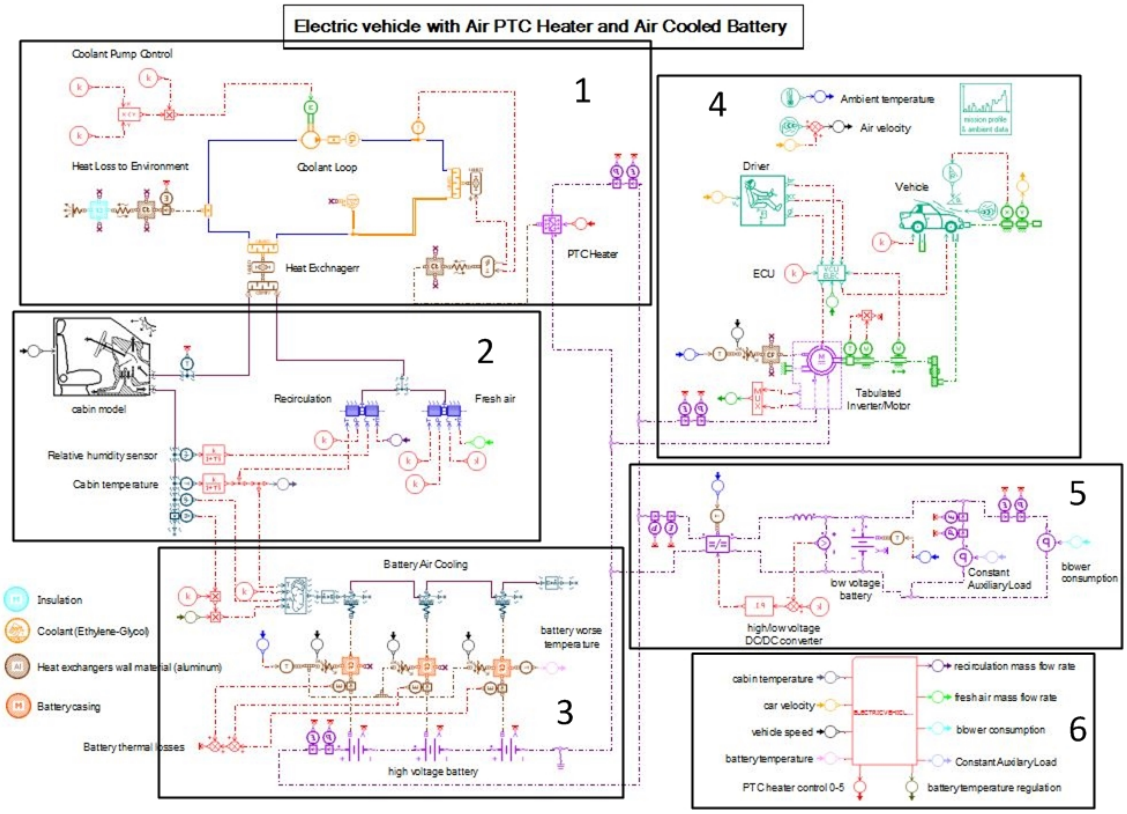

Figure 3.1: AMESim model for baseline simulations.

mechanical components are in green, the driver and vehicle are in turquoise and the thermal components are in brown. The various subsystems are outlined and numbered. A single motor, front wheel drive powertrain was assumed for this research. Subsystem '1', contains the coolant loop, the high voltage PTC heater, and the heat exchanger which connects the heater loop to the vent air. The main research of this thesis involves making changes to this subsystem and seeing how they affect the overall vehicle performance and range. Subsystem '2', contains the blower and the cabin model, which can be seen in detail in Fig. 3.2. The cabin model, which was pre-built and made available by the AMESim software, contains a thermal network connecting the cabin air to the ambient air through a variety of paths and materials. The

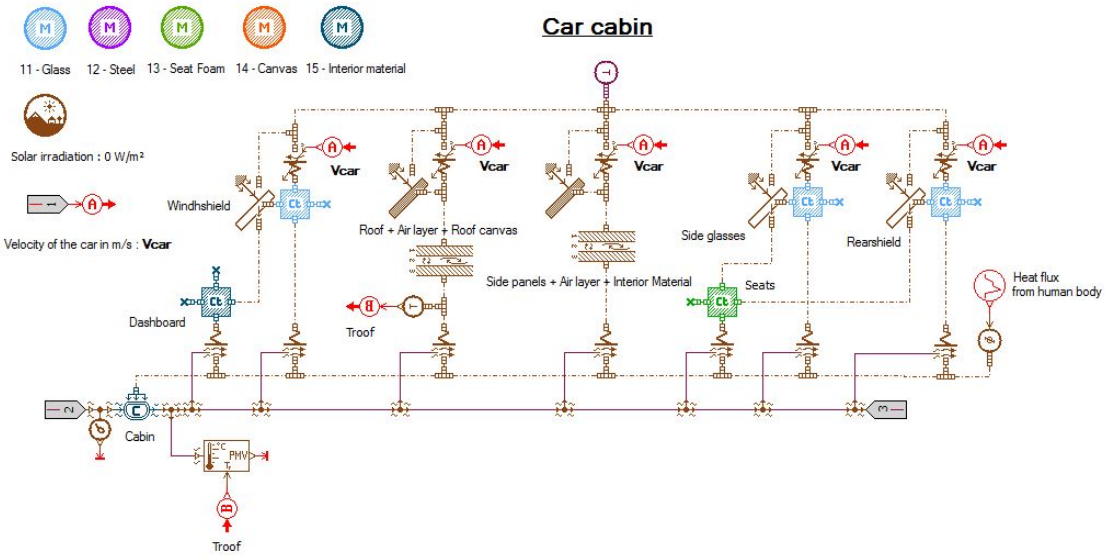

Figure 3.2: AMESim model of the vehicle cabin.

cabin model is well described in [30]. Other strategies for electric vehicle thermal load modeling can be found in [31], [32], [33] and [34]. For this research, the solar irradiance was considered to be 0 W/m^2 for all cases representing overcast of night driving scenarios. However, it should be noted that the sun can have tremendous impact on vehicle heating. The blower pushes a fixed 20 % fresh air into the heat exchanger located in subsystem '1' while 80% is recirculated cabin air. The air mass flow rate into the cabin is 0.12 kg/s. The 20% leaving the cabin is diverted to the battery for heating. The blower consumption was held constant throughout all simulations, regardless of ambient temperature, cabin temperature or otherwise. A representation of the HVAC system can be seen in Fig. 3.3. Subsystem '3' contains the high voltages battery pack and the air cooling components. The electric motor, the inverter, the driver model and the vehicle model can be found in subsystem '4'. This is where the drive cycle is input, and a torque is requested and generated by the motor. The

motor and inverter are modelled by a single block which contains a look-up table for the efficiency. The motor/inverter combined efficiency is a function of speed, voltage, torque and temperature and an efficiency map at a single voltage and temperature can be seen in [30]. Subsystem '5' represents the low voltage network. It includes

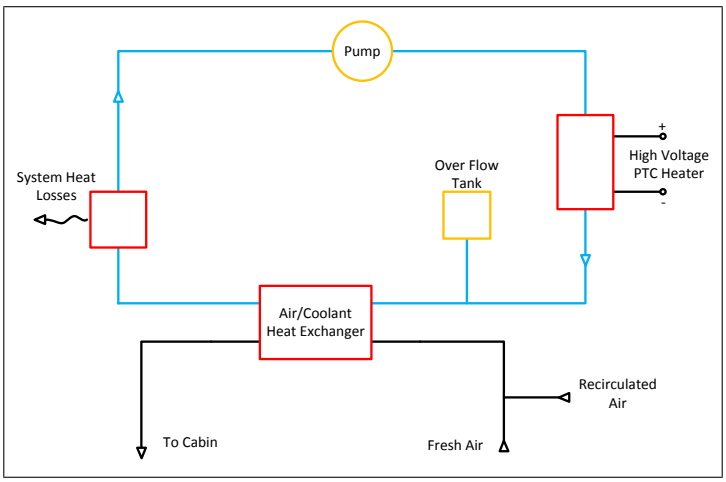

Figure 3.3: Baseline coolant loop representation.

a DC/DC converter, a 12 volt battery, and a representation of the various auxiliary loads. Finally, subsystem '6' contains most of the controls for the HVAC system. The PTC heater has a step output with preset stages. The heater used in the model is a 5 stage heater with the first four steps being 1 kW and the final stage 2 kW, giving this a maximum output of 6 kW. It is controlled based on the difference between the desired and actual cabin temperature. The controller uses 5 triggers each with different high and low-threshold values. For more information on subsystems '2' to '6', refer to [30]. The controller layout can be seen in Appendix A. The coolant loop was built in AMESim with all pipe components having a diameter of 25 mm with a length of 100 mm. Both heat exchangers had 0.5 litres involved in the heat transfer process giving a total coolant volume of 2 litres. All external temperatures were set

to ambient with initial internal temperatures set the same. Now that the model was constructed, parametrization was necessary.

3.2 Representing the Nissan Leaf

The AMESim model was initially a representation of an arbitrary electric vehicle. However, many parameters were then specified to match those of the Nissan Leaf battery electric vehicle (BEV) parameters. The important parameters and overall architecture of the model are very similar to the Leaf and when compared to data from Argonne National Laboratories [6], the model performed very well. Details on the model accuracy are provided in Section 3.3. The Nissan Leaf has a single traction motor with cabin heating coming from a coolant based PTC heater [35], consistent with the model. Some of the relevant Leaf specification used in the AMESim model are summarized in Table 3.1. The 24 kWH hour battery was modelled with an initial state-of-charge of 80 % in order to represent the pack utilization. The nominal cell voltage was selected to be consistent with the Nissan Leaf at 3.75 volts with a maximum of 4.2 volts [36, 37]. The only parameters changed in AMESim's vehicle cabin model was the cabin volume to 2.6 m^3 and the solar irradiance to 0 W/m^2. For more information on the parametrization of the AMESim vehicle model, see the figures in Appendix A.

Table 3.1: Some relevant Nissan Leaf specifications.

Parameter	**Value**
Vehicle Mass	1704.5 kg [6]
Battery Capacity	24 kWh claimed [6]
Pack Utilization	80 % [36]
Battery Voltage	360 V [36]
Battery Chemistry	Li-ion [6]
Auxiliaries	180 W [38]
Final Gear Ratio	7.938 [38]
Air Penetration Coefficient	0.32 [39]
Vehicle Active Area	2.276 m^2 [39]
Cabin Volume	2.6 m^3 [40]
Tire Size	205/55 R16 [41]

3.3 Model Verification

Argonne National Laboratory produced some experimental results of the 2011 Nissan Leaf found in [6]. The vehicle was run on a 4WD chassis dynamometer for several drive cycles. As a reference, a UDDS drive cycle was run at 72 °F (22.2 °C) with the heater off. Additionally, a UDDS at 20 °F (-6.7 °C) was conducted where the vehicle was cold soaked (kept in -6.7 °C ambient conditions) for 12 hours and then the heater was set to 'auto mode' with a desired cabin temperature of 72 °F (22.2 °C) during the cycle. The effect of the wind speed was emulated by a large fan which matched the vehicle speed according to [6]. A cold soaked, UDDS cycle was simulated in the

baseline AMESim model at -6.7 °C with the desired cabin temperature set to 22.2 °C in an effort to emulate the experimental tests performed in [6]. Fig. 3.4 shows the energy consumption rates of the two cases from Argonne along-side the simulated results from the AMESim model. The original plots from AMESim can be seen in Appedix B. It should be noted that in the original plots, the legend possess three relevant entries which are the "base", "heater" and "cold" energy consumptions. The "Energy Lost from Battery" seen in Fig. 3.4 was assumed to be the same as the "cold" consumption, since it was unclear which of the three legend entries contained the blower energy and auxiliary energy in [6].

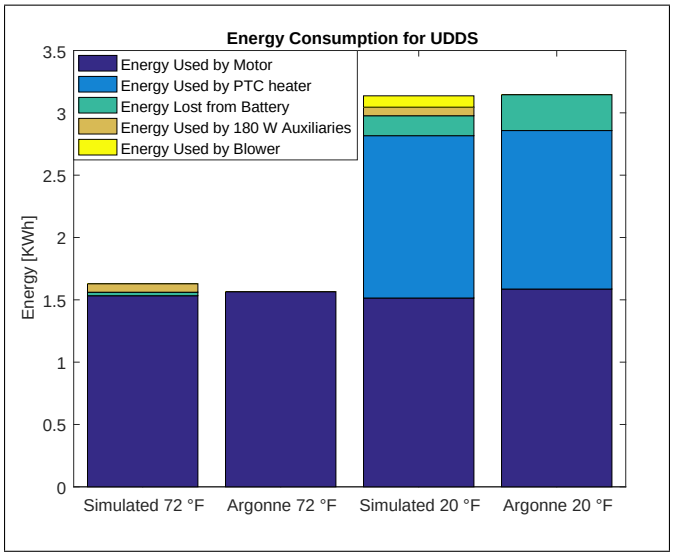

Figure 3.4: Simulated energy consumption rate in kWh during a cold start UDDS at -7 °C (20 ° F) and 22 °C (72 °F) compared to experimental results from [6].

Table 3.2: Comparison of simulated energy usage during UDDS to the experimental results from Argonne [6].

Temperature [°C]	Simulated Energy [kWh]	Experimental Energy [kWh]	Error [%]
22.2	1.63	1.57	3.68
-6.67	3.14	3.15	0.32

The simulations matched the experimental results from Argonne very closely. An error of less than 4% was achieved in both the mild and cold temperature case. These results are summarized in Table 3.2. Also provided by Argonne was the temperature profiles during various cycles. The UDDS temperature profiles for the mild case are compared in Fig. 3.5 and for the cold case in Fig. 3.6 on the same temperature scale. At 22.2 °C, the all temperatures are relatively constant as no heating or cooling is occurring. Therefore, as expected, the simulated and experimental results correlate very closely in Fig. 3.5. At -6.7 °C however, a warming of the vent air, cabin air and battery can be observed from Fig. 3.6. While the vent temperature in the simulation was less when compared to Argonne's results, the cabin temperature and battery temperature showed strong similarities. Both the simulation and experimental results from Table 3.2 take about 700 seconds to reach the desired 22.2 °C Fahrenheit and the final battery temperatures are both very close to 10 °C. More results and the original data from [6] can be found in Appendix B. It was concluded based on this evidence that the model created in AMESim adequately represented the Nissan Leaf performances.

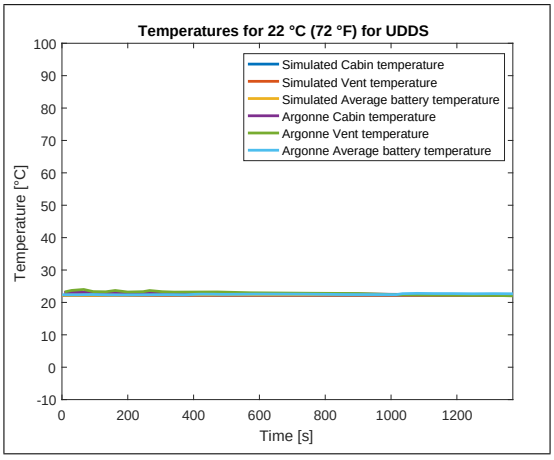

Figure 3.5: Simulated temperature in °C during a UDDS cycle compared to experimental results from [6] at 22 °C (72 °F).

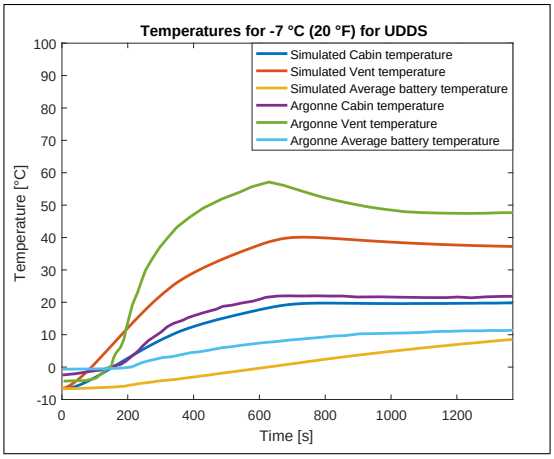

Figure 3.6: Simulated temperature in °C during a cold start UDDS compared to experimental results from [6] at -7 °C (20 °F).

Chapter 4

Benchmark Simulations of Energy Consumption and Thermal Behaviour of a Representative Electric Vehicle

This chapter will summarize some of the results obtained from simulating the baseline model in different driving conditions.

4.1 Baseline Simulation

Once the model was created and confirmed to be a sufficiently accurate representative EV model, simulations were performed to produce baseline of results over a wide range of temperatures and drive cycles. The results included in this section use the UDDS and HWFET cycles at ambient temperatures ranging from -30 °C to 20 °C. Both hot start (HS) and cold start (CS) cycles were simulated as well as 3 UDDS cycles in sequence in order to capture the effect of a longer cycle. A cold start scenario would occur when the vehicle is sitting in cold climate for an extended period of time such that all vehicle components reached ambient temperature. A hot start scenario, on the other hand, would occur when the vehicle cabin and battery have been preconditioned to a temperature of 20 °C. The drive cycles can be seen in Fig.

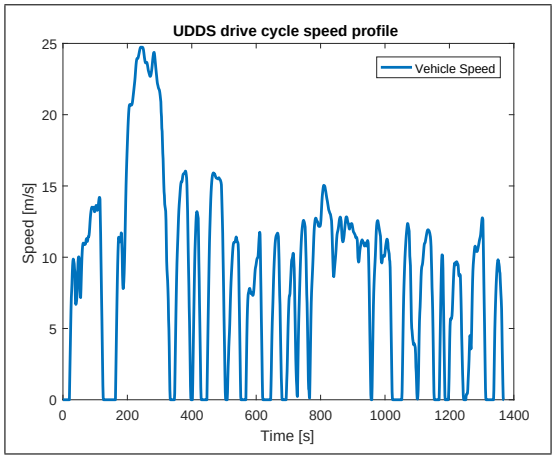

(c) UDDS drive cycle.

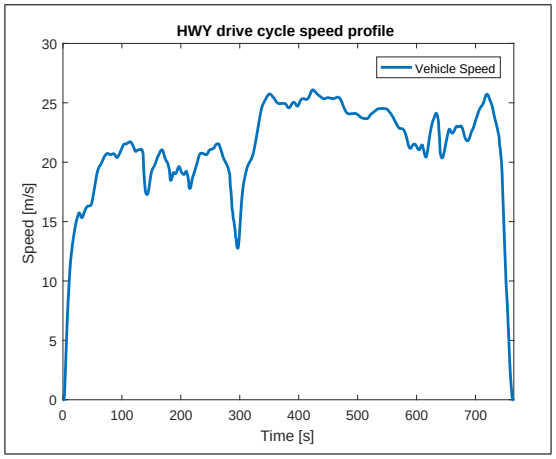

(d) UDDS drive cycle.

Figure 4.1: Velocity profiles used for baseline simulation.

4.1. The UDDS cycle, also called FTP-72, simulates an urban route lasting about 1372 seconds over a distance of about 12.07 km [42]. The HWFET simulates a highway driving route lasting about 765 seconds over a distance of about 16.45 km [43].

4.1.1 Detailed Cold Start City Drive Cycle Results

The baseline AMESim model generates in excess of 1000 different result vectors for each simulation. This section will provide a more detailed view of a cold start, UDDS simulation while for other cycles only an overview of the simulation is provided with the detailed results included in the appendix. Fig. 4.2 shows the amount of

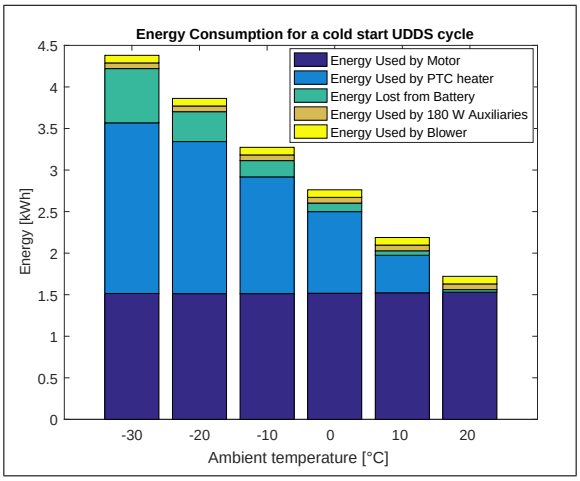

Figure 4.2: Simulated energy consumption in kWh during the UDDS.

energy used by different components at various temperatures during the CS UDDS cycle. The energy input to the motor is nearly constant at all temperatures and includes all losses in the inverter, motor, powertrain and wheels. The heating energy and battery losses increase significantly as temperature decreases. Under these city conditions, the battery losses make up as much as 1/4 of the additional energy demand at cold temperatures. Table 4.1 summarizes the range implications of the temperature decrease. Based on this model, relative to the 20 °C case, the -30 °C case has nearly one-third of the range. This highlights the major challenge of range reduction in cold conditions.

Table 4.1: Cold start city drive cycle (UDDS) simulation results

Tamb [degC]	SOC used [%]	Energy Used [kWh]	Range [km]
-30	17.2	4.38	55
-20	15.1	3.86	62
-10	12.7	3.27	74
0	10.6	2.76	89
10	8.4	2.19	114
20	6.4	1.63	148

The following plots will show some temporal behaviours of the model. In Fig. 4.3, the energy consumption trajectory is displayed for the same cold start, UDDS cycle. In other words, the figure displays the energy leaving the battery as electrical

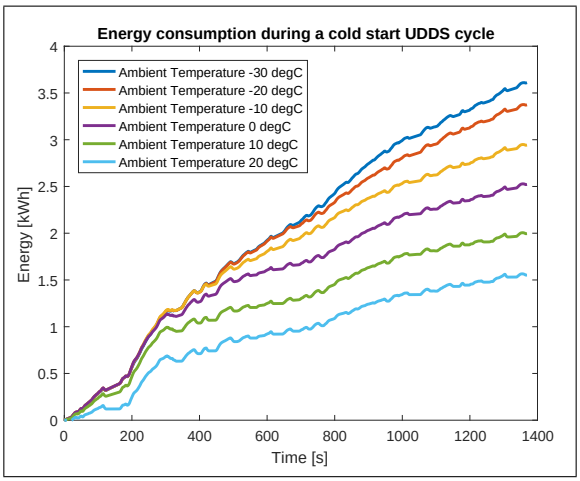

Figure 4.3: Simulated cumulative energy consumption in kWh during the UDDS.

current as a function of time. The general trend as time progresses is upward with the slope changing as a result of either a change in velocity demand or a change in PTC heater demand. The small negatively sloped segments are where the vehicle is

decelerating and some regenerative breaking occurs. It is clear from Fig. 4.3 that at colder temperatures, considerably more energy is used. In Fig. 4.4, the temporal battery energy loss is displayed. The battery energy losses in the UDDS can make

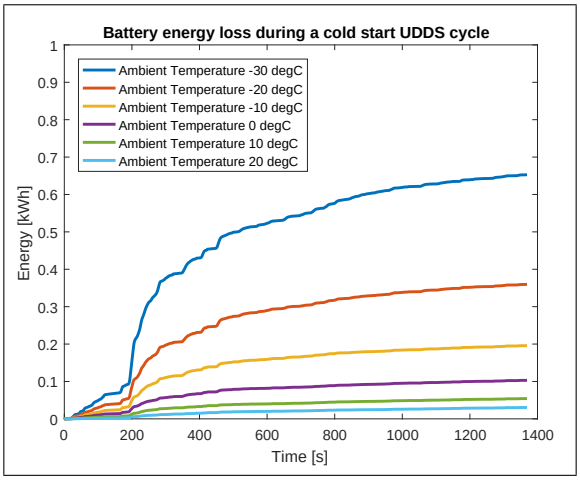

Figure 4.4: Simulated cumulative energy loss in kWh during the UDDS.

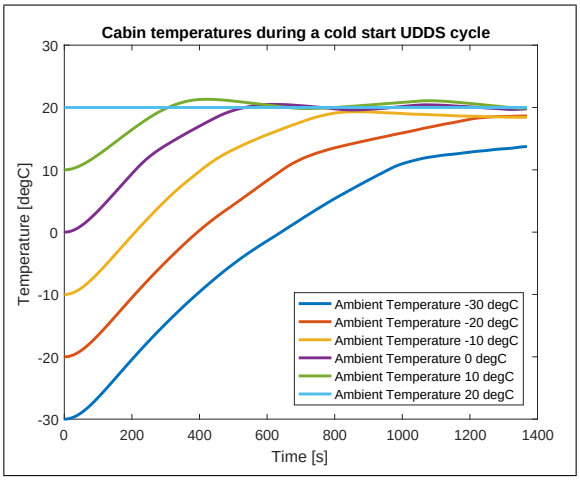

Figure 4.5: Cabin temperature during the UDDS.

up as much as 16 % of the total energy used during the cycle. Fig. 4.5 shows the cabin temperature during one cold start, UDDS cycle. During this 23 minute, 12 km cycle, all but the -30 °C case reached a desired temperature of 20 °C. Fig. 4.6

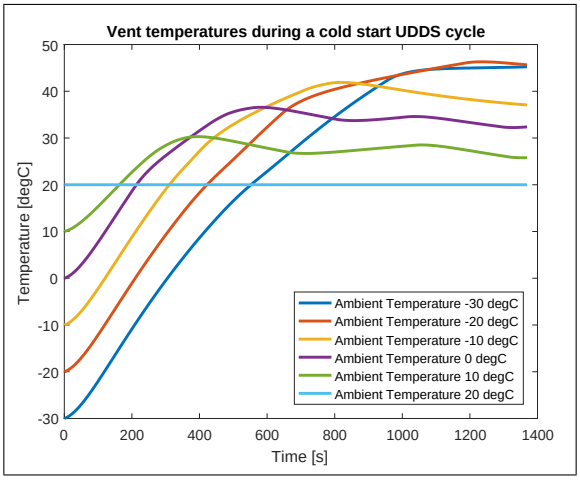

Figure 4.6: Vent temperature during the UDDS.

displays the vent temperature. This is the temperature of the air entering the cabin. At lower ambient temperatures, since the heat demand is lower, the vent temperature is lower and at 20 °C, there is no heating required and therefore the vent temperature is constant. Fig. 4.7 presents the average battery temperature throughout the cycle.

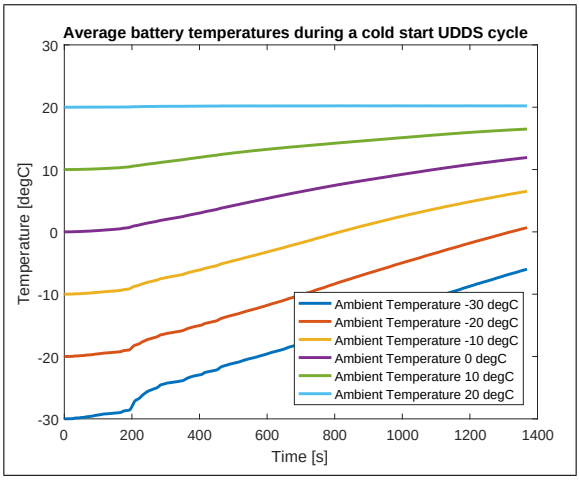

Figure 4.7: Average battery temperature during the UDDS.

Since this architecture uses the cabin air to heat the battery, the heating process is slow. Finally, Fig. 4.8 shows the battery internal resistance for one of three modules

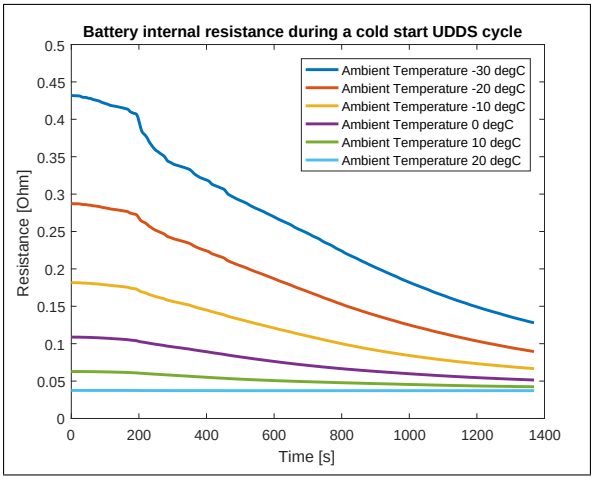

Figure 4.8: Battery internal resistance during the UDDS for one of three battery modules connected in series.

at various ambient temperatures. The total pack resistance is three times larger at any temperature, since the modules in the model are series-connected. At -30 °C, the internal battery resistance is roughly 10 times larger than at 20 °C. This is ultimately the driving factor in increased battery energy losses at low temperatures. The average heat consumption for the CS UDDS cycle at -30 °C was about 5 kW.

4.1.2 Cold Start Highway Drive Cycle

Fig. 4.2, displays a bar chart of the energy used during a CS highway drive cycle. Since this cycle is much more demanding than the UDDS and only about half as long, the impact of the cold temperature appears to be less significant. The highway cycle demands almost 3 kWh for traction, 1.25 kWh for heat, and has 1 kWh of battery losses, while the UDDS uses 1.5 kWh, 2 kWh and 0.75 kWh for these respective tasks. Though the HWY cycle uses roughly 7 % more energy per second for heating, the traction energy in the HWY cycle is much higher than in the UDDS and therefore the

range impact of cold weather for the HWY cycle is reduced. The simulations have shown that the HWY range can be nearly cut in half, where as the city cycle was cut to almost a third. However, it is interesting to note that the battery losses in the highway cycle make up a larger portion of the additional load when compared to the city cycle. Table 4.2 show the ramifications that a heating system can have on SOC, energy use and therefore range at low temperatures. The average heat consumption for the CS HWY cycle at -30 °C is roughly 5.6 kW. More results from this cycle can be found in Appendix C.

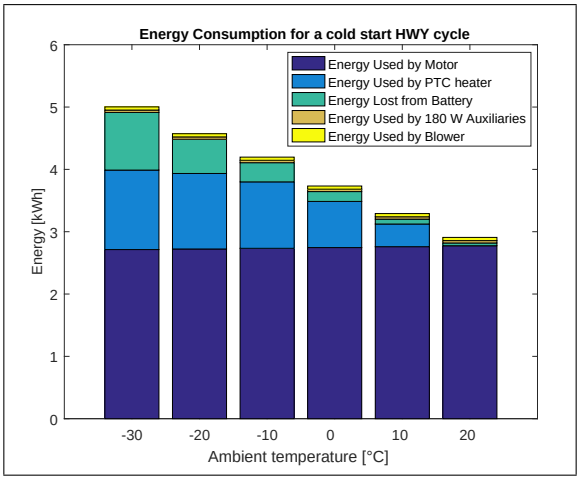

Figure 4.9: Simulated energy consumption in kWh during a CS HWY cycle.

Table 4.2: Cold start highway drive cycle (HWFET) simulation results

Tamb [degC]	SOC used [%]	Energy Used [kWh]	Range [km]
-30	20.1	5.00	64
-20	18.4	4.57	70
-10	16.8	4.20	77
0	14.9	3.73	87
10	13.1	3.29	99
20	11.5	2.86	113

4.1.3 Three UDDS Cycles Back-to-Back

The purpose of testing cycles back to back is to observe the steady state behaviour, the variation in energy consumed per cycle and to observe the impact of a longer cycle. It was determined that three cycles were needed to achieve steady state operation. The cycle is depicted in Fig. 4.10. Firstly the cold start scenario will be discussed.

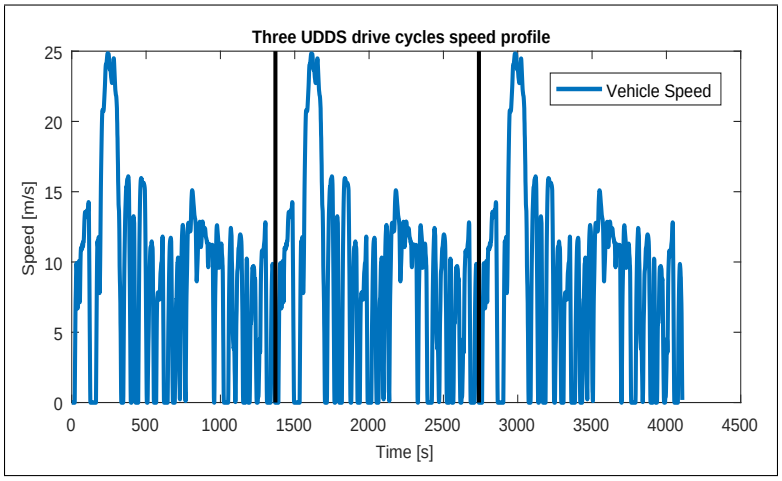

Figure 4.10: Velocity profile during three UDDS drive cycles.

This would suggest that the first UDDS cycle would be identical to the previously discussed CS UDDS cycle, and then the vehicle model enters a second cycle with the initial conditions matching the final conditions of the first cycle, and so on. As the simulation enters the second cycle, the vehicle is partially warmed and therefore requires less energy to heat the cabin and battery. The initial warm up phase in the first cycle is not necessary in the second cycle. The energy distribution at -30 °C for the three UDDS cycles can be seen in Fig. 4.11. This plot shows a significant

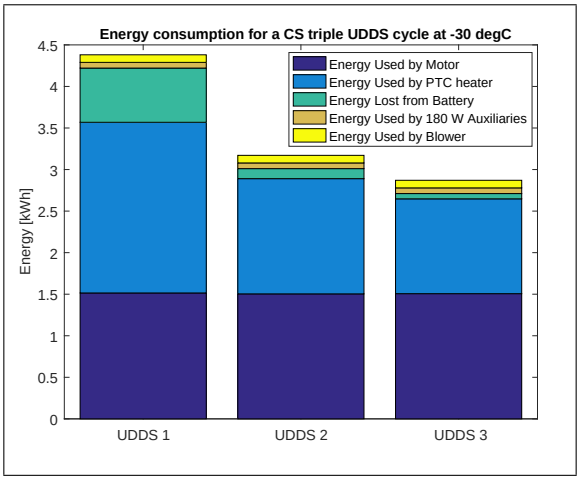

Figure 4.11: Simulated energy consumption in kWh during a CS triple UDDS cycle per cycle at -30 °C.

reduction in battery losses and heating requirements from cycle one to two. Starting the drive cycle with a warm vehicle can reduce energy use by up to 30 %. These energy savings directly, positively impact the range of the vehicle. Table 4.3 shows the SOC, energy used and range of the vehicle model based on the CS triple UDDS cycle. Similar to the previous sections, the range was calculated by assuming the exact cycle is repeated. Multiplying the distance travelled during the triple cycle by the ratio of available SOC to used SOC provides an estimate of the vehicle range. Essentially, the amount of times the vehicle could undergo the identical cycle based

on SOC is multiplied by the distance of one cycle.

Table 4.3: Three cold start city drive cycle (UDDS) simulation results

Tamb [degC]	SOC used [%]	Energy Used [kWh]	Range [km]
-30	41.8	10.42	68
-20	36.7	9.28	77
-10	32.2	8.18	88
0	27.7	7.12	103
10	22.9	5.99	124
20	19.6	4.93	148

It is known from [36], that the leaf only uses 80 % of available energy in order to protect the battery pack. Since this is a representative EV model of the Leaf, the same 80 % was used throughout all simulations for range calculations. Three UDDS cycles have a distance of about 36 km and in the -30 °C case, the SOC used was slightly more than half of the available SOC therefore yielding a range of 68 km. Fig. 4.12 and Fig. 4.13 show the temporal cabin temperature and battery temperature over the three cycles. These figures display that the vehicle model has reached a steady state cabin temperature and a nearly steady state battery temperature. They also provide an idea of initial temperatures for the second and third UDDS cycle the cabin and battery. Additional simulation results for this cycle can be seen in Appendix D.

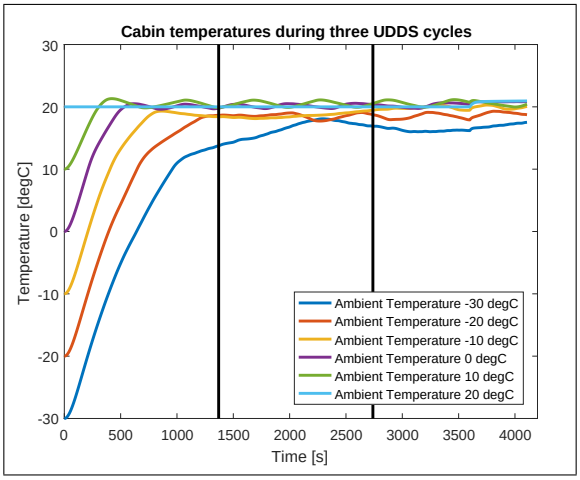

Figure 4.12: Cabin temperature during three UDDS cycles.

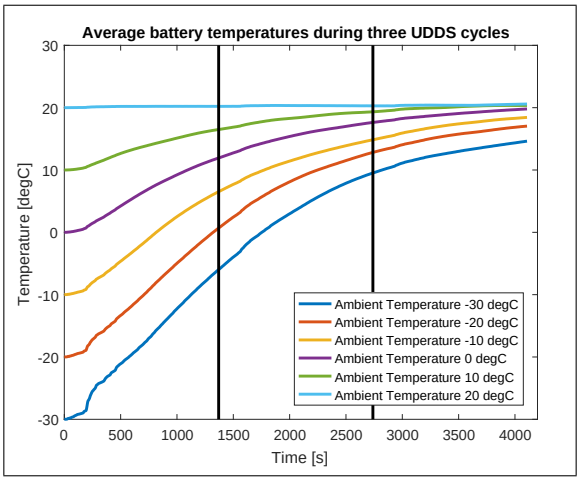

Figure 4.13: Average battery temperature during three UDDS cycles.

Considering the impact that a warm vehicle had on the second and third cycle, a HS triple UDDS cycle was simulated. A hot start cycle represents a preconditioned vehicle where the initial cabin and battery were set to 20 °C. The initial coolant temperature was set between 20 °C and 40 °C depending on the ambient temperature. These initial coolant values were selected based on the final coolant temperatures of the cold start cycles. It was assumed that while the vehicle was being preconditioned

(warmed up), the coolant would be warmed as well. The initial coolant temperatures used in the HS simulations can be seen in Table 4.4. From Fig. 4.14, it can be observed that at -30 °C, the three cycles are using very similar energy. The minor discrepancy from cycle to cycle is due to the coolant temperature being slightly higher than its steady state value. If the initial coolant temperature was slightly decreased, the three cycles would converge.

Table 4.4: Initial coolant temperatures for HS simulations.

Ambient Temp. [°C]	Initial Coolant Temp. [°C]
-30	40
-20	36
-10	32
0	28
10	23
20	20

On the same scale as the CS figures, Fig. 4.15 and Fig. 4.16 show the temporal temperature distribution of the cabin and battery respectively. In this hot start case, the deviation from the desired 20 °C is minor over the duration of the cycle at all temperatures. Table 4.5 provides an overview of the SOC and energy used during the cycle as well as the range based on this cycle. More results from the HS triple cycle can be found in Appendix E. Recognizing the impact of back to back cycles, and steady state heat demand, the following sections examine at a hot start scenario for both UDDS and HWY cycles.

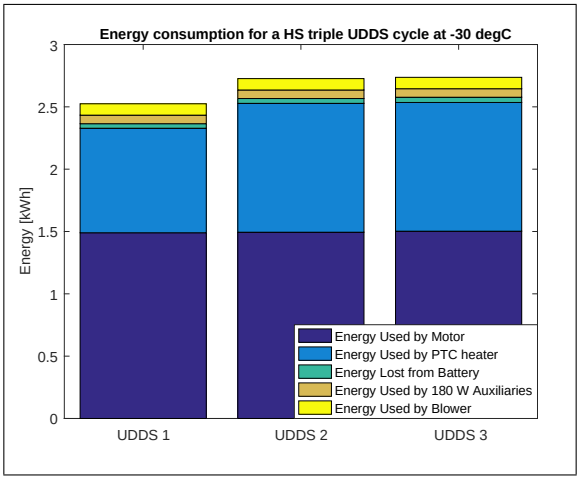

Figure 4.14: Simulated energy consumption per cycle in kWh during a HS triple UDDS cycle.

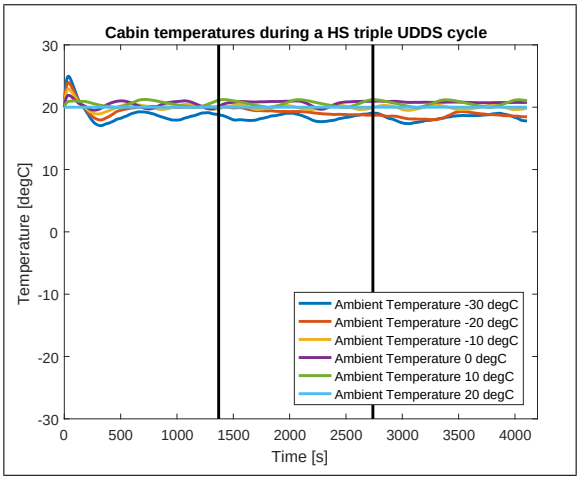

Figure 4.15: Cabin temperature during a HS triple UDDS cycle.

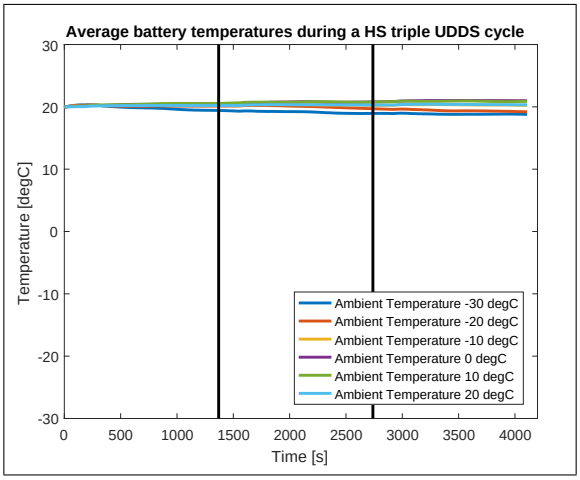

Figure 4.16: Average battery temperature during a HS triple UDDS cycle.

Table 4.5: HS triple city drive cycle (UDDS) simulation results

Tamb [degC]	SOC used [%]	Energy Used [kWh]	Range [km]
-30	31.4	8.00	91
-20	28.8	7.38	99
-10	26.4	6.83	108
0	24.0	6.23	119
10	21.2	5.57	134
20	19.7	4.94	148

4.1.4 Hot Start City and Highway Drive Cycles

The "hot start" indicates that the vehicle has been preconditioned. This means that before a driver leaves, while the vehicle is plugged in for charging, it can use grid energy to activate the heater and warm the vehicle. This reduces the start-up energy requirement for thermal comfort. Fig. 4.17 displays the energy used by the

vehicle at different temperatures during a hot start UDDS. The HS UDDS uses 44 % less energy as the CS UDDS at -30 °C. Similarly, as seen in Table 4.6, the range is significantly improved at -30 °C from 55 km to 98 km. Preconditioning nearly completely eliminates the battery losses (-0.8 kWh) and cuts the heating demand by more than half (-1.2 kWh). Additional simulation results for this cycle can be seen in Appendix F.

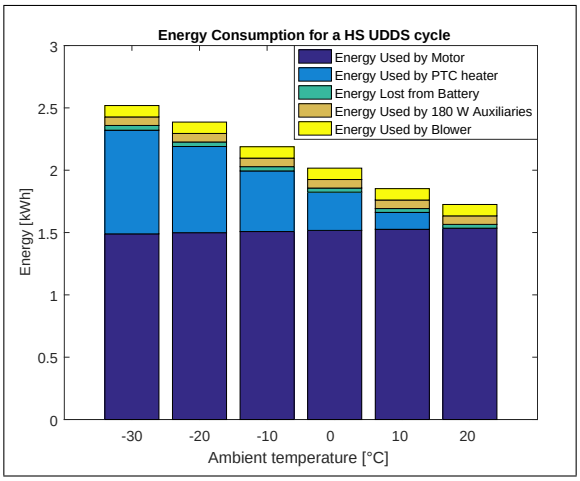

Figure 4.17: Simulated energy consumption in kWh during the HS UDDS.

Table 4.6: Hot start city drive cycle (UDDS) simulation results

Tamb [degC]	SOC used [%]	Energy Used [kWh]	Range [km]
-30	9.6	2.52	98
-20	9.1	2.39	104
-10	8.3	2.19	114
0	7.6	2.02	124
10	6.9	1.85	137
20	6.4	1.63	148

The HS HWY drive cycle was also performed in the baseline simulation model. The results can be seen in Fig. 4.18 and Table 4.7. The energy savings are not quite as significant as the UDDS cycle primarily due to the decrease in cycle duration. A 30 % reduction in energy use is still observed with a range improvement from 64 km to 97 km as compared to the CS HWY. Similar to the city cycle, these savings come from the elimination of the battery losses (-1 kWh) and the reduction of the heating demand by half (-0.6 kWh). Additional simulation results for this cycle can be seen in Appendix G.

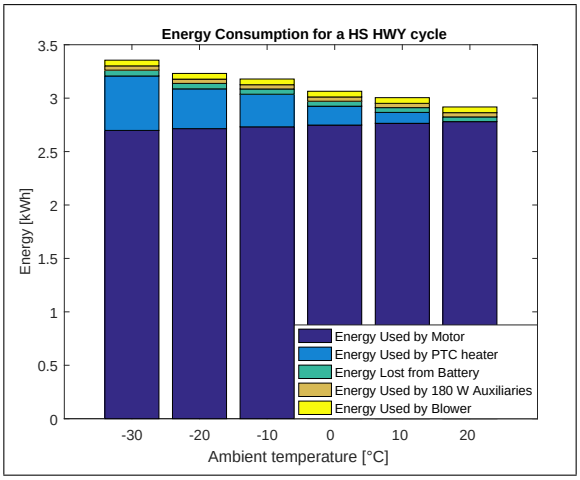

Figure 4.18: Simulated energy consumption in kWh during the HS HWY.

Table 4.7: Hot start highway drive cycle (HWFET) simulation results

Tamb [degC]	SOC used [%]	Energy Used [kWh]	Range [km]
-30	13.3	3.36	97
-20	12.8	3.23	101
-10	12.6	3.18	103
0	12.1	3.06	107
10	11.9	3.00	109
20	11.5	2.86	113

4.2 Baseline Summary

In summary, the baseline model was tested with both high way and city driving cycles at bot hot and cold initial conditions. The ranges at different temperatures and cycles were gathered and are compared in Table 4.8. It is clear from this table that no matter which cycle, the range drops significantly with temperature. The slope of the decrease in range, as a function of temperature, was significantly reduced when the vehicle model was preconditioned to 20 °C.

Table 4.8: Range comparison for baseline simulations.

	Cold Start Range [km]			Hot Start Range [km]		
Tamb	UDDS	HWY	3 UDDS	UDDS	HWY	3 UDDS
-30 °C	55	64	68	92	94	91
-20 °C	62	70	77	99	96	99
-10 °C	74	77	88	109	99	108
0 °C	89	87	103	120	104	119
10 °C	114	99	124	138	109	134
20 °C	148	113	148	148	113	148

Since the majority of EV owners are primarily concerned with range, the range was the primary focus for the baseline results. However, range is an extrapolated value which can be difficult to calculate in vehicles possessing a thermal storage system. A better explanation of the difficulties of range calculation when TS systems are present can be found in Section 7.3. For this reason, the consumption was used as the primary unit of comparison for judging the effectiveness of the TS system. A summary of the baseline consumption values can be seen in Table 4.9. After the baseline was established, a thermal storage system was developed and simulated in an attempt to improve vehicle range. This model is discussed in Chapter 5 and its results in Chapter 6.

Table 4.9: Consumption comparison for baseline simulations.

	Cold Start Consumption [Wh/km]			Hot Start Consumption [Wh/km]		
Tamb	UDDS	HWY	3 UDDS	UDDS	HWY	3 UDDS
-30	371	310	294	213	207	225
-20	327	283	261	201	200	208
-10	277	260	230	185	196	192
0	233	231	200	170	189	175
10	185	203	169	156	186	157
20	145	180	146	146	180	147

Chapter 5

Thermal Storage Concept for Heating Electric Vehicles

This chapter will describe the thermal storage system that was implemented in the EV model as a potential solution to the range reduction challenge that is present in cold weather conditions. The changes made to the baseline model will be outlined as well as the heat loss and weight implications of installing thermal storage in an EV.

5.1 Thermal Storage System Concept

As discussed and shown in simulations in Chapter 4, the range loss due to cold climates can be significant. The task of this research was to devise a solution to mitigate the large variations in range from summer to winter climates. Thermal storage was investigated as an affordable and simple alternative to using battery energy to heat the cabin. The additional components required to implement this system are a storage medium and containment, as well as a means to extract and deliver heat to the cabin. Several different configurations are possible depending on the storage material selected. For simplicity, the storage medium was kept consistent with the vehicle coolant (50/50 ethylene-glycol/water), and the storage containment was selected to be a chamber in line with the existing coolant loop. This system would require no additional coolants, storage mediums, or interconnecting coolant loops. The system may possibly require a slightly larger pump depending on the size of the tank though this was not investigated as part of this research.

While plugged in, both the electrical battery and the "thermal battery" get fully charged. Just before departure, the vehicle and battery are pre-conditioned to a desired temperature using grid energy. In cold weather conditions, instead of drawing battery energy for electrical heating, as is done in current EVs, the cabin heat comes from the thermal storage. Depending on the length and type of the drive cycle, the installed thermal storage can partially or fully offset the heating demand thus improving range. Once the coolant temperature falls below what is required to maintain cabin temperature, a standard PTC heater comes online to assist in the vehicle heating.

During a cold start situation where a driver leaves their EV outside, not connected

to the grid for an extended period of time, the coolant temperature would drop to ambient temperature. This is problematic since, now, in order to heat the cabin, the PTC heater must use enough energy to first heat all of the thermal storage. Valves were introduced to divert the coolant around the thermal storage in the event of a cold start up, in order to rectify this potential issue. A representation of the HVAC system, adjusted to accommodate thermal storage with the coolant by-pass, can be seen in Fig. 5.1. A by-pass valve was also added to the air side of the system. This

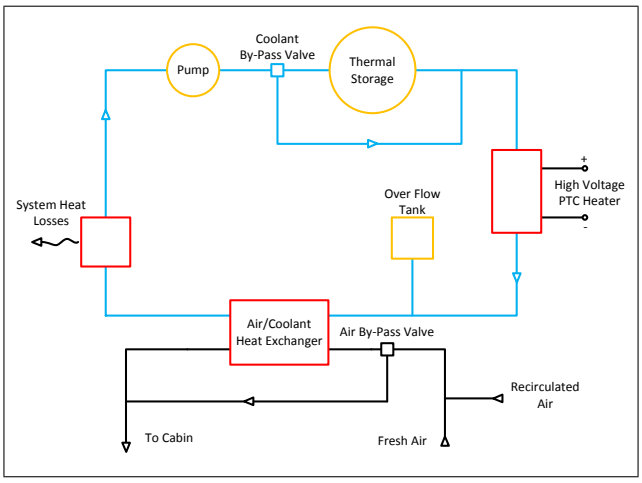

Figure 5.1: HVAC system with thermal storage representation.

was done in order to ensure that the vent temperature remained below the maximum safe level. In order to increase energy density, the coolant temperature was initially higher than in the baseline case, and maintaining the same flow rates would produce vent temperatures in excess of 55 °C. This concern was rectified by adding a valve to the air-side of the heat exchanger, diverting a certain percentage of the air around the heat exchanger in order to lower the vent temperature. This lowered the vent air temperature by only heating some of the air and then mixing it back together with the diverted air.

5.2 Thermal Storage System Model in AMESim

Now that the concept and strategies involved with the thermal storage system had been established, the modelling was started. The model used in the baseline simulations discussed in Chapter 4 and all its parameters were kept unchanged with the exception of the coolant loop and the heating controls. The changes are highlighted in Fig. 5.2. The main alterations to the model include the addition of: the "chamber" for the thermal storage, the coolant diverging loop and its valves, the air by-pass loop and valve, and of the controls for the new valves. The thermal storage diverging loop was simple to control. If the coolant started at a temperature below the minimum coolant requirement, the thermal storage would be removed from the system. However, the air by-pass was much trickier to control. Since minor fluctuations in the air mass flow rate drastically altered the heat flow rate to the air, a step-wise controller could no longer be used. A proportional-Integral (PI) controller was used. The reference input to the controller was the difference between the desired and actual cabin temperature. The proportional gain was 1E-03 and the integral gain was 5E-04. The PI output was then corrected to increase faster for smaller thermal storage masses. The PTC controls remained very similar in terms of when to turn the various stages on and off. What had changed was that while the air valve was diverting less than 80 percent of the air to the heat exchanger, the PTC heater was off. Once the air by-pass valve control signal surpassed 80 percent, indicating the coolant temperature was approaching too low of a temperature to accommodate the heating demand, the PTC heater was switched on and controlled by monitoring the difference from the desired to actual cabin temperature. Fig. 5.3 shows the control signal and heater output alongside coolant and cabin temperature during a HS UDDS cycle with 14 kg

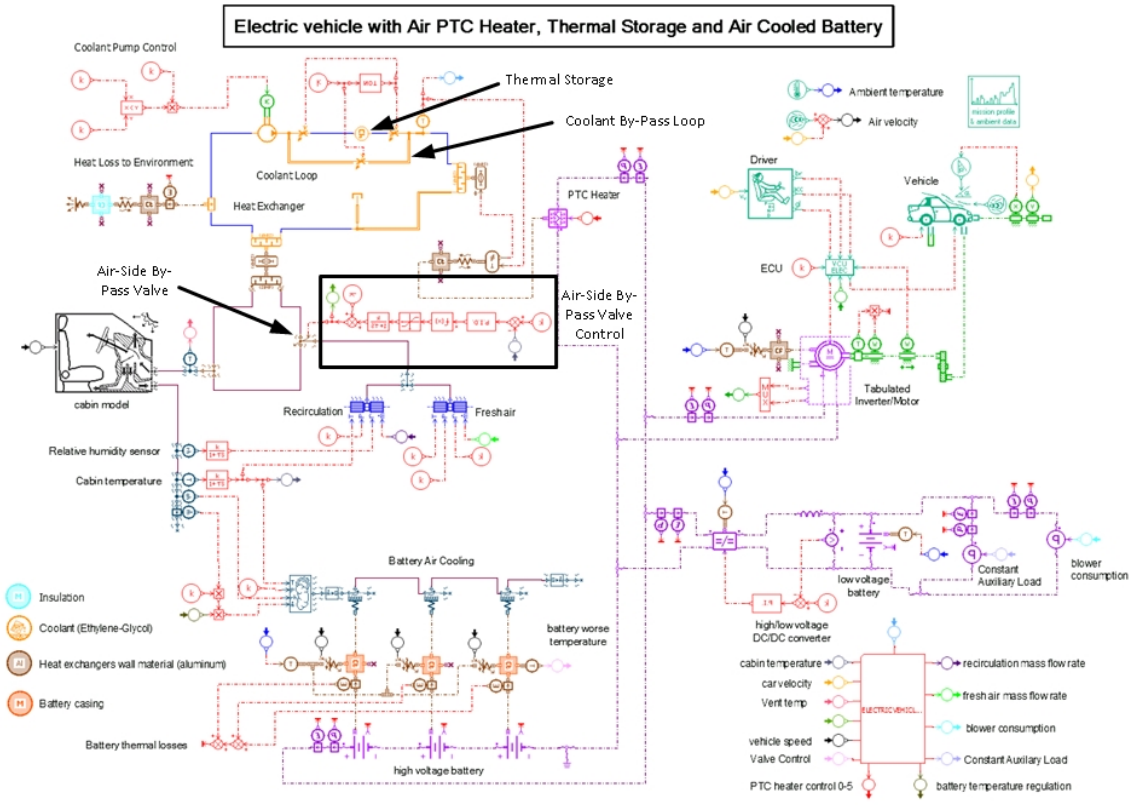

Figure 5.2: AMESim model for thermal storage simulations.

of thermal storage. As the coolant temperature decreases, the PI controlled air valve increases the mass flow rate of the air diverted through the heat exchange in order to maintain the heat flow to the cabin. Very subtle changes in the cabin temperature, not observed on this plot, cause the PI increase the air valve control signal. In the figure, at 80 % valve signal, the PTC heater switches on, which slows the coolant temperature decrease. The valve signal continues to 100 %. In some cases, allowing the valve to completely open before turning on the heater, would cause a drop in the cabin temperature. To avoid this, the heater was switched on at 80 % instead of 100 % valve control during all of the TS simulations.

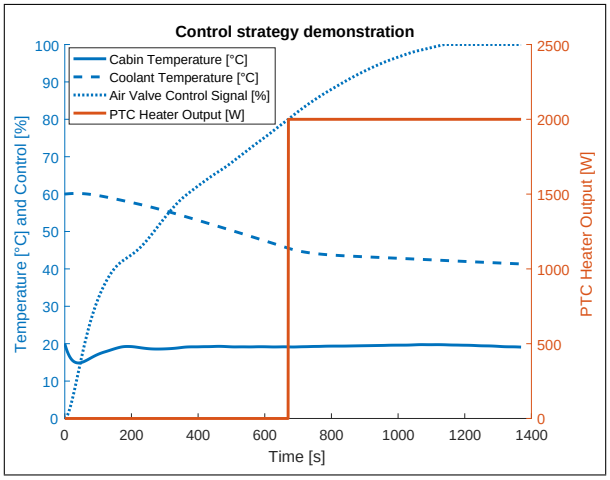

Figure 5.3: Plot of the control signal, PTC heater output, cabin temperature and coolant temperature for a HS UDDS cycle with 14 kg TS to show control operation.

5.3 Cost, Size and Weight Implications

In most vehicles, the main concerns are cost, weight and size. There has always been a push to make things lighter, smaller and cheaper. This is no different for electric vehicles only that the weight concern is slightly diminished as compared to ICE vehicles due to the addition of regenerative breaking. In order to accelerate additional mass, more energy is required which is then stored as kinetic energy. In conventional vehicles, this additional energy is wasted as heat loss from the friction in the breaks. However in vehicles with regenerative breaking capabilities, some of the added energy can be re-captured and pushed back to the battery pack. The impact of adding mass to electric vehicles with and without regenerative breaking can be seen in Fig. 5.4 and Fig. 5.5 respectively. In these figures, a standard HS UDDS cycle was ran at -30 °C and at 20 °C with no other changes in the simulations other than the mass of the vehicle. The mass of the vehicle was varied from 1705 kg (0 kg added mass) to 1865 kg (160 kg added mass), for a maximum mass increase of almost 10 %.

With regenerative breaking, the range decreased by 3.9 % and 2.5 % for the 20 °C and -30 °C cases respectively. This is consistent with [44] where an EV was estimated to have a 4.1 % range extension for a 10 % mass reduction. With no regeneration, these numbers increased to 5.1 % and 3.7 % respectively. This consistent with [45], where a 10 % weight reduction on a gas powered vehicle yielded a 4.8 % range improvement on the same drive cycle. In either case, regenerative breaking or not, the effect of increasing the mass by 10 % appeared to have limited impact on the vehicle range, though lesser in vehicles with regenerative breaking, especially when compared the positive impact of the thermal storage mass on cold temperature performances as shown in the following Chapter.

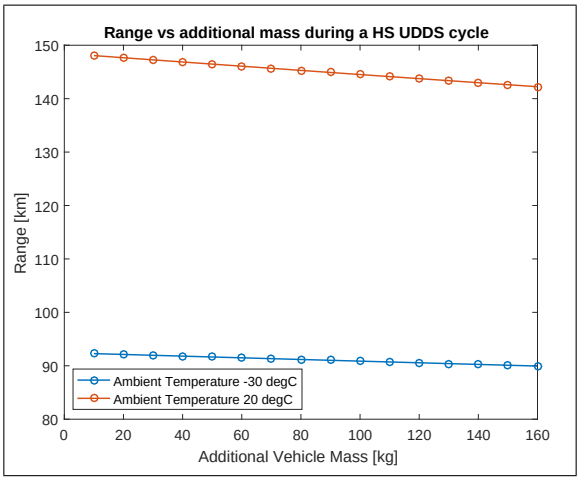

Figure 5.4: Effect of adding mass to electric vehicle range with regenerative breaking.

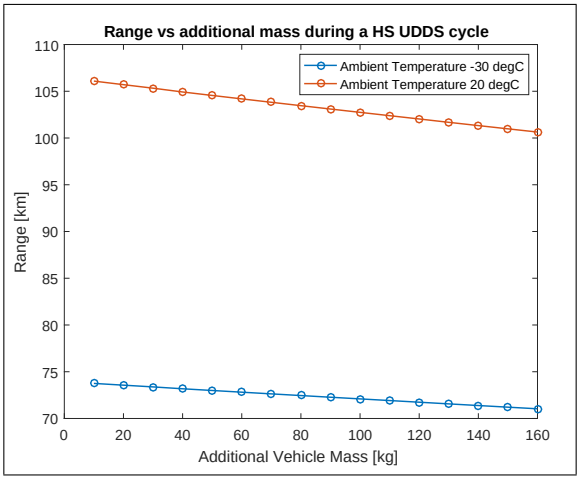

Figure 5.5: Effect of adding mass to electric vehicle range with no regenerative breaking.

Therefore the primary concerns are size (packaging) and cost. The cost of coolant is very low and the implementation into the system would be quite simple and low cost. The volume, however presents an interesting challenge. Without knowing specifics about the engine compartment volumes in electric vehicles, it is difficult to speculate on whether or not a certain tank volume would fit. However, a coolant based thermal storage tank has the benefit of being extremely flexible when it comes to volume. Oddly sized shapes and pipes can easily be used to fit around various components and accommodate tight spaces. The low cost, geometry-flexible nature of the coolant thermal storage tank further separates it as the best energy storage option for the EV heating application. For the purpose of the following loss calculations, a cylindrical tank is assumed.

5.4 Thermal Storage Heat Losses

In the AMESim model, only the heat losses in the coolant pipes are included. This is consistent between both the baseline and the thermal storage models. Due to its complexity, the losses from the thermal storage tank itself, were not included in the model. However, the following calculations were performed to show the potential impact. Several assumptions were made during these calculations. In general, a worst case (highest losses) approach was taken. A thermal model of the tank was first approximated and is represented in Fig. 5.6. The tank was assumed to have a half inch aluminum casing with one inch of polystyrene insulation. For a worst case approximation, it was assumed that the inside wall of the tank was at the same temperature as the coolant. The thermal network was extracted from the diagram in Fig. 5.6 and is detailed in Fig. 5.7. With a low emissivity outer insulation surface, radiation losses were assumed to be negligible in the calculations.

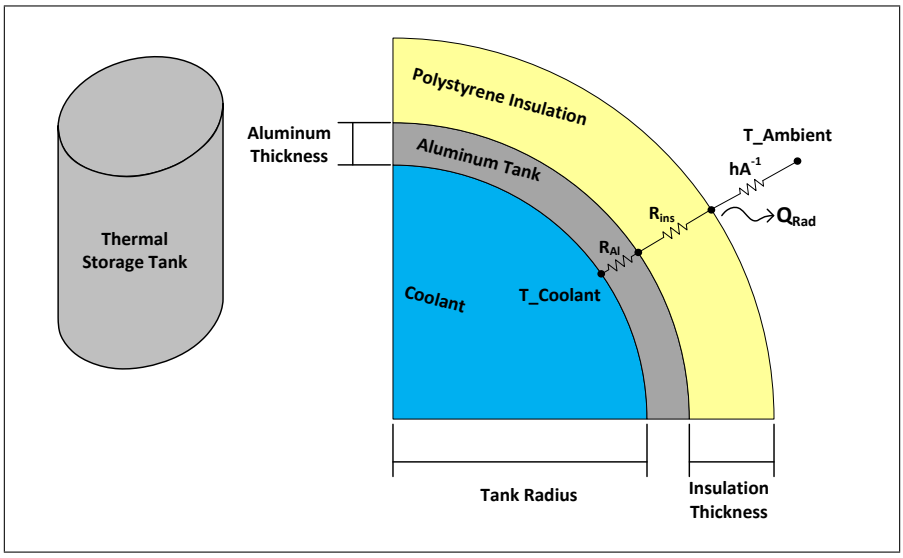

Figure 5.6: Representative thermal storage tank thermal network (not to scale).

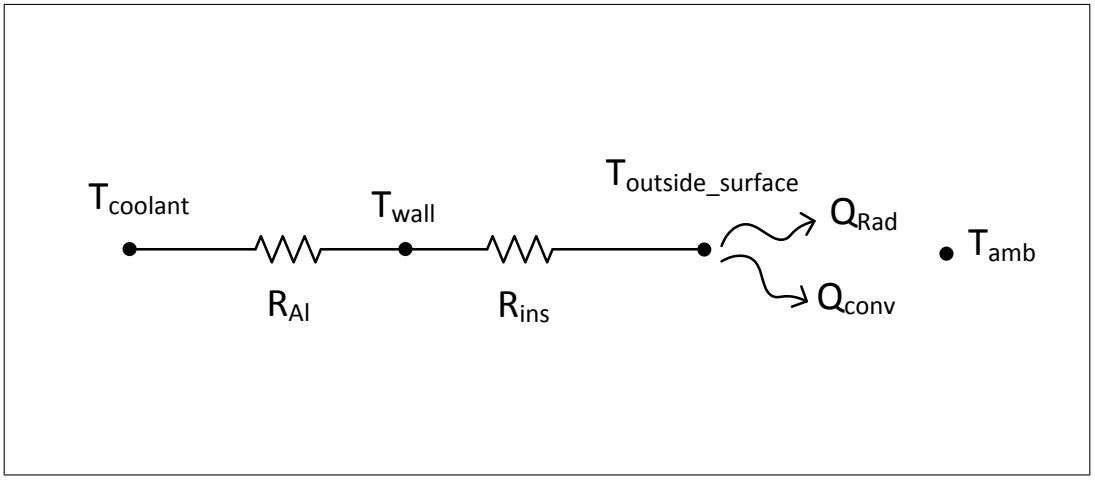

Figure 5.7: Thermal storage tank thermal network.

An assumed convection coefficient of 12 W/m^2 k was used for the calculation. This convection coefficient was selected by assuming 10 W/m^2 k due to natural convection and adding a calculated 2 W/m^2 k due to the circulating air. The conditions for the following calculation include are a 160 L tank, 588 mm tank diameter, 1.63 m^2 of tank surface area, -30 °C ambient temperature and 80 °C coolant temperature. The inner wall temperature and the ambient temperature were known. The thermal resistances were determined and the heat loss was calculated. The diameter used for the calculation was one which equalled the cylinder height thus minimizing the tank surface area and the losses. The heat losses (Q_{conv}) can be calculated by Equation 5.1 where the total resistance (R_{total}) is calculated from 5.2.

$$Q_{conv} = \frac{(T_{surface} - T_{ambient})}{R_{total}} \tag{5.1}$$

$$R_{total} = \frac{1}{SA_{tank}} \cdot \left(\frac{L_{ins}}{k_{ins}} + \frac{L_{al}}{k_{al}} + \frac{1}{h_{conv}} \right) \tag{5.2}$$

Performing these calculations with the above-listed conditions yielded a total heat loss

of 227 W. If the coolant temperature remained at 80 °C for an entire triple UDDS cycle (1 hour 9 minutes long), the total energy lost would be 0.259 kWh. On a HS triple UDDS with no TS, the total energy used is roughly 8 kWh, with 3 kWh of heat energy. This indicates in a worst case scenario, the heat loss from the tank is 5.2 % of the cycle energy and 8.6 % of heat energy used at -30 °C.

The actual losses would be less due to several of the conservative assumptions made. Particularly, due to the fact that the coolant temperature does not remain constant throughout the simulation, but in fact decreases constantly. Assuming an average coolant temperature of 60 °C during the cycle (instead of 80 °C), reduces the losses by about 25 W or 12 %. A sensitivity analysis was performed to see which other parameters had a significant impact on the tank losses. Each parameter in Table 5.1 was varied by 30 %, in the direction which increased the losses. Ambient temperature and coolant temperature have a clear impact, but also the tank dimensions and the type and thickness of its insulation. The convection coefficient is perhaps the parameter with the most uncertainty. Based on the sensitivity analysis, it has a relatively small impact on the heat losses due to the dominance of the insulation on the thermal resistance. Even when increasing the convection coefficient by 100 % to 25 W/m^2 k, the loss increase was limited to 13 W or 6 %. To summarize, the worst case of heat loss from the thermal storage tank was less than 10 % of the used heat and thus was neglected at this stage of the AMESim modelling. Intuitively, the impact of the heat loss would be reduced at warmer ambient temperatures and lower coolant temperatures. Additionally, it can be further reduced with thicker insulation.

Table 5.1: Sensitivity analysis on heat loss from thermal storage from a reference of 160 L tank at 80 °C in -30 °C ambient conditions. Parameters were varied +/- 30 %.

Parameter	Base Value	Heat Loss Increase
Convection Coefficient (h)	12 [W/m^2 k]	6 W
TS Tank Volume	160 [L]	44 W
TS Tank Diameter	588 [mm]	18 W
Ambient Temp.	-30 [°C]	19 W
Coolant Temp.	80 [°C]	50 W
Thermal Conductivity of Insulation (k)	0.036 [W/m k]	60 W
Thermal Conductivity of Aluminum (k)	205 [W/m k]	No Effect
Insulation Thickness	25.4 [mm]	60 W
Aluminum Thickness	12.7 [mm]	No Effect

The variation in coolant temperature of a tank subjected only to thermal losses for an 8 hour period can be seen in Fig. 5.8. The respective instantaneous heat loss can be seen in Fig. 5.9. These plots present the transient heat loss calculations where the initial heat loss at 0 minutes for 160 kg of storage, is the same as what was previously calculated. The purpose of these plots is to show the temperature drop of an tank sitting in a parking lot for 8 hours and to show to reduced losses on the smaller tanks.

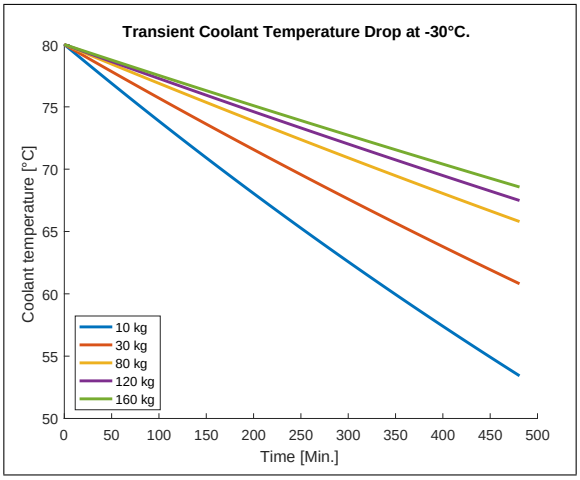

Figure 5.8: Coolant temperature of a transient heat loss calculation for a tank starting at 80 °C in -30 °C air.

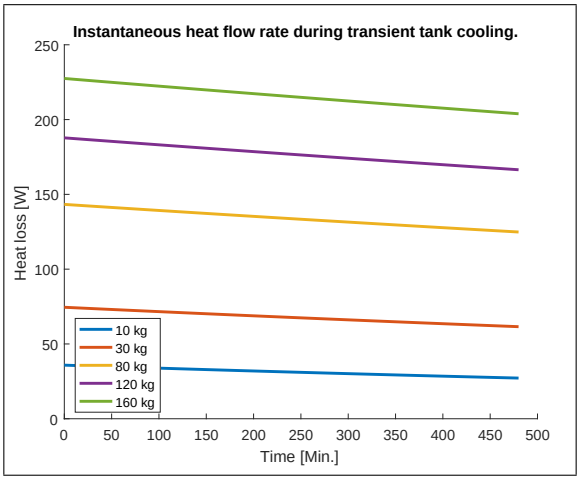

Figure 5.9: Instantaneous heat loss by a coolant tank starting at 80 °C in -30 °C air.

An assumption made by the AMESim storage tank is that the tank has a uniform temperature. The following will show the validity of this assumption using a HS UDDS cycle with 30 kg of TS at -30 °C. Fig. 5.10 shows the coolant temperature in blue from AMESim during the cycle. This has a very smooth profile due to the uniform tank assumption. However, with a large tank, the temperature inside is not

necessarily all uniform. The coolant at the top of the tank starts at 60 °C begins to flow through the heat exchanger where a temperature drop occurs. This coolant then returns to the bottom of the tank where due to its lower density, will remain at the bottom until the entire volume of the tank is cycled through the system. At this point, the tank output temperature will then step down. Fig. 5.10 additionally shows the temperature steps assuming a perfectly stratified tank with a system flow rate of 12 L/minute. With this flow rate, the 30 L tank turns over once ever 2.5 minutes. The largest step size from this plot is observed to be between 2 and 3 °C. This means that at any given time the actual tank temperature could be 2 or 3 °C higher than the temperature calculated based on the uniform tank assumption.

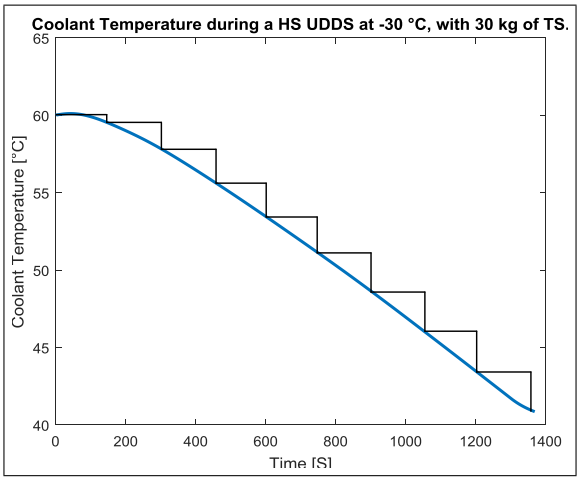

Figure 5.10: Coolant temperature during a HS UDDS cycle at -30 °C with 30 kg of TS.

Fig. 5.11 shows the heat flow to the cabin as a function of coolant temperature for two cases. A simulation was performed where the air valve was diverting a constant temperature and flow rate of air to the heat exchanger. The coolant temperature was then slowly increased from 30 to 80 °C by the PTC heater and the relationship

between the heat flow to the air and the coolant temperature was plotted in red. The blue curve shows the same relationship but with the data coming from the UDDS cycle simulation. Due to the controls, the two lines look very different. After an initial start-up phase where the PI controller is ramping up, the heat flow rate begins to flatten out. Ignoring the 57-60 °C range, from this plot an uncertainty of 2-3 °C in coolant temperature (due to the uniform tank assumption) leads to a heat flow error of up to 200 W. The uncertainty is less than 10 % of the average heat flow rate of 2.5 kW for the cycle. This indicates that for the 30 kg TS tank, the assumption of a uniform tank temperature is reasonable. However, at higher tank masses, this assumption begins to have greater errors. A different tank assumption could be used to better represent a real scenario however, AMESim does not have another tank model available. Other, more realistic tank models, could include some degree of stratification in the tank. The uniform assumption is conservative, indicating that it is possible that a smaller tank could accomplish the same heating task.

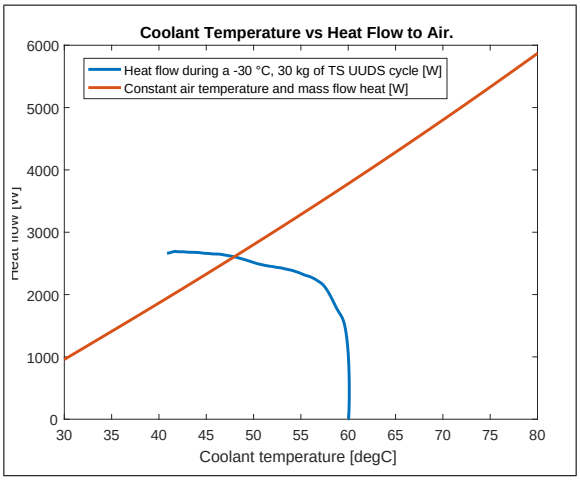

Figure 5.11: Heat flow to cabin as a function of coolant temperature.

Chapter 6

Electric Vehicle Range Impact of Thermal Storage Systems

This chapter will discuss the hot start thermal storage model results across several different ambient temperatures, thermal storage masses, initial tank temperatures and drive cycles.

6.1 Thermal Storage Simulation Overview

With the added components discussed in the previous chapter, the thermal storage model was simulated. The CS cycles were initially run however, since the thermal storage was also cold at the beginning of the cycle, the valves in the model adjusted to divert coolant around the thermal storage. This essentially created the same system as in the baseline case. The results of the thermal storage model and baseline model were nearly identical and thus were not discussed. The results in this chapter are of the hot start condition. The simulations begin with both the battery and cabin at 20 °C. The thermal storage tank and coolant start at either 60 °C or 80 °C depending on the simulation. The ambient temperature is swept from -30 °C to 20 °C in increments of 10 °C and the thermal storage mass is varied between 2 kg and 30 kg for the UDDS and HWY cycles and between 10 kg and 160 kg for the triple UDDS cycle. It should be noted that as the mass of the thermal storage increases in the model, the mass of the vehicle increases by the same amount such that the negative impact of increased vehicle mass is captured. The same city (UDDS) and highway (HWFET) cycles were used for the simulations in addition to a triple UDDS cycle to examine the performance of the thermal storage system.

6.2 Thermal Storage Results - Hot Start UDDS Cycle

For this cycle, the TS mass was increased from 0 kg to 30 kg. Steps of 2 kg were used and the results are plotted in Fig. 6.1 and Fig. 6.2. In Fig. 6.1, the consumption based on each simulation was plotted. At 20 °C, the heat demand is zero and therefore

the optimal consumption occurs with no additional mass. Similarly, at 10 °C, no additional mass is required during the cycle. The amount of 60 °C coolant in the lines (roughly 2 L) is enough to fulfil the low heating demand. However, when the

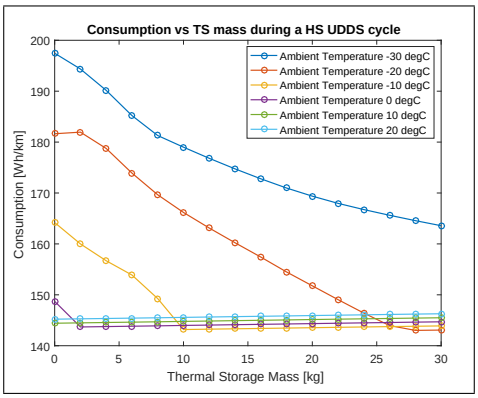

Figure 6.1: EV consumption vs. thermal storage size at varying ambient temperatures at an initial coolant temperature of 60 °C during a HS UDDS cycle.

ambient temperature is 0 °C, a minimum 2 kg of additional thermal storage is required to meet the heat demand. This number increases to 10 and 28 kg for the -10 °C and -20 °C respectively. At -30 °C, it can be observed that even 30 kg of 60 °C thermal storage is not enough, and the PTC heater is required regardless of added mass. Fig. 6.2 shows the PTC heat energy used during one cycle. All ambient temperature cases reach zero PTC heat energy at a certain thermal storage mass except the -30 °C case. After further simulations, it was determined that 60 kg of thermal storage was required to ensure all heating demands were met at -30 °C. Looking closer at Fig. 6.1, it can be seen that the 20 °C consumption is higher than the other ambient temperature cases once enough TS mass is added. It was initially hypothesized that the 20 °C case would have the best consumption regardless of the added mass due to the marginally higher battery losses at lower temperatures. However, when looking at the energy consumption breakdown seen in Fig. 6.3 and Table 6.1, an understanding

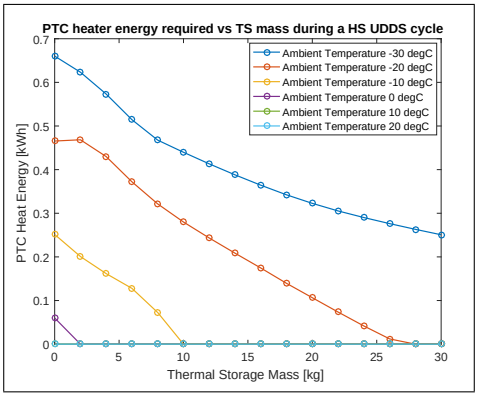

Figure 6.2: PTC heater load vs. thermal storage size at varying ambient temperatures at an initial coolant temperature of 60 degC during a HS UDDS cycle.

of why this hypothesis was incorrect can be observed. The primary reason is due to the improved motor and inverter efficiency at lower temperatures. Previously, this concept was not observed. With the inclusion of thermal storage, the heater draw from the battery disappears, thus revealing the small change in traction load. A 3.1 % change in traction energy converts to an improvement in consumption of 5 Wh/km. A secondary reason for the incorrect hypothesis was the absence of change in battery losses with temperature. Since the battery was preheated and the cycle is only 23 minutes long, the battery temperature does not change significantly.

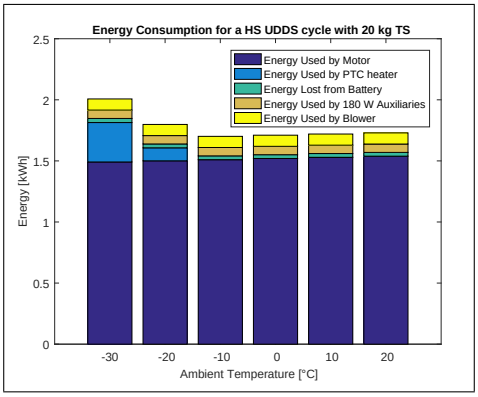

Figure 6.3: Energy breakdown for a HS UDDS with 20 kg of TS at an initial coolant temperature of 60 degC.

Table 6.1: Energy break down for a HS UDDS with 20 kg of TS at an initial coolant temperature of 60 degC.

	Energy Consumed by [kWh]				
Tamb [°C]	Traction	PTC Heat	Battery Losses	Auxiliary	Blower
-30	1.491	0.323	0.0335	0.0684	0.0913
-20	1.501	0.107	0.0317	0.0684	0.0913
-10	1.510	0	0.0310	0.0684	0.0913
0	1.520	0	0.0309	0.0684	0.0913
10	1.529	0	0.0309	0.0684	0.0913
20	1.539	0	0.0308	0.0684	0.0913

The same simulations were performed for an initial thermal storage temperature of 80 °C. A significant improvement is noticed when comparing Fig. 6.4 to Fig. 6.1. The -30 °C case is satisfied with only 20 kg of thermal storage. The PTC heater energy required as thermal storage increases can be seen in Fig. 6.5. From this plot, it can be confirmed that no heat energy is supplied by the PTC heater with 20 kg or

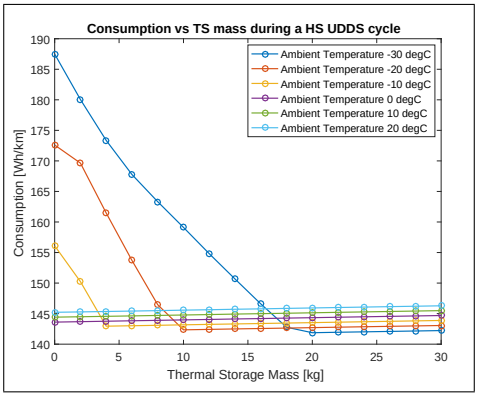

Figure 6.4: EV consumption vs. thermal storage size at varying ambient temperatures at an initial coolant temperature of 80 degC during a HS UDDS cycle.

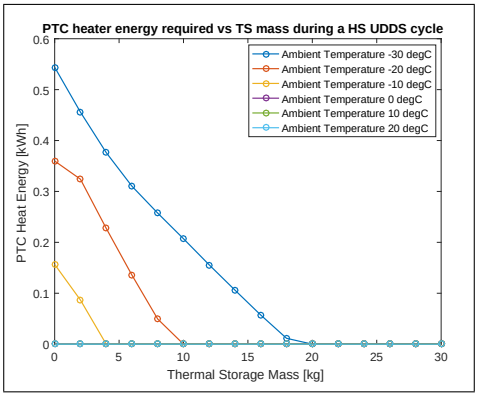

Figure 6.5: PTC heater load vs. thermal storage size at varying ambient temperatures at an initial coolant temperature of 80 degC during a HS UDDS cycle.

more of thermal storage. Looking back to Table 4.6, in Chapter 4, the consumption based on the HS UDDS cycle of the baseline model was from 213 Wh/km at -30 °C to 146 Wh/km at 20 °C. Due to the discrepancy in initial coolant temperatures, the 0 kg of added thermal storage case does not match the baseline case in the colder temperature simulations. The additional 25 °C of initial coolant temperature combined with refined controls decrease the consumption by about 16 Wh/km in -30 °C according to the model, bringing the baseline to 197 Wh/km. In either case, at 60 °C coolant temperature, an decrease in consumption of 17 % or 23 % is observed

at -30 °C, depending on the selected baseline. At 80 °C, the consumption can be decreased by 24 % or 33 % with 20 kg of thermal storage at -30 °C. This decrease in consumption does however come at a minor consumption increase of 1.4 % at ambient temperatures between 0 and 20 °C.

6.3 Thermal Storage Results - Hot Start HWFET Cycle

Similar to the HS UDDS cycle, the same 0 kg to 30 kg thermal storage masses were investigated for the HS HWY cycle. Fig. 6.6 displays the consumption of each simulation as ambient temperature and thermal storage mass change. Due to the more aggressive nature of the highway cycle, the impact of the energy savings appears to be less significant. This is strictly due to the fact that the heat energy makes up a smaller portion of the total energy used and so the reduction in heat energy makes a smaller impact on the vehicle consumption. The decrease in consumption due to the addition of the 60 °C thermal storage at an ambient temperature of -30 °C was from 207 Wh/km (baseline model) to 176 Wh/km. At 0 kg of additional thermal storage, the consumption based on the HS HWY cycle was 196 Wh/km. This indicates a consumption decrease of either 10 % or 15 %. This is about half of the impact that the thermal storage had on the UDDS cycle consumption. Fig. 6.7 presents the heat energy drawn from the battery by the PTC heater at the various TS masses. The trends of the constant ambient temperature lines are different in some cases. This is likely due to the sensitivity of the controllers. Since the PTC heater is a step-wise device, constant (or linear) trends are sometimes difficult to achieve. In the case of the

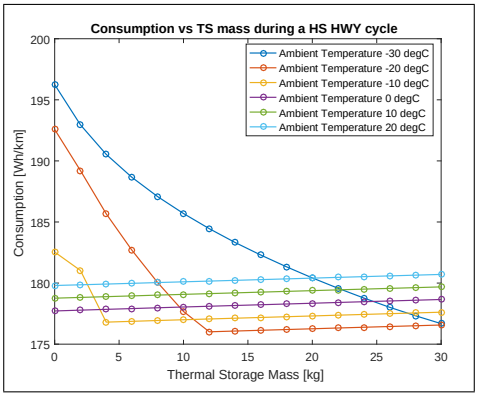

Figure 6.6: EV consumption vs. thermal storage size at varying ambient temperatures at an initial coolant temperature of 60 degC during a HS HWY cycle.

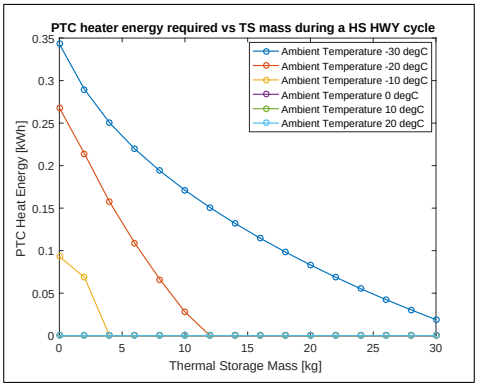

Figure 6.7: PTC heater load vs. thermal storage size at varying ambient temperatures at an initial coolant temperature of 60 degC during a HS HWY cycle.

-30 °C line, in both 60 °C coolant cycles discussed so far, it appears to asymptotically approach zero PTC heat energy. This is due to the fact that the PTC heater comes online once the air valve control signal reaches 80, the coolant then begins to heat up and as a result the air valve signal begins to increase at a slower rate. In a lot of these cases, the air valve never reaches a fully open state and not all TS energy is used. The reason this control was introduced was to ensure that the cabin temperature did not drop too far before the PTC heater brought the coolant temperature back up to minimum levels. Fig. 6.8 shows the energy breakdown of the 20 kg of thermal

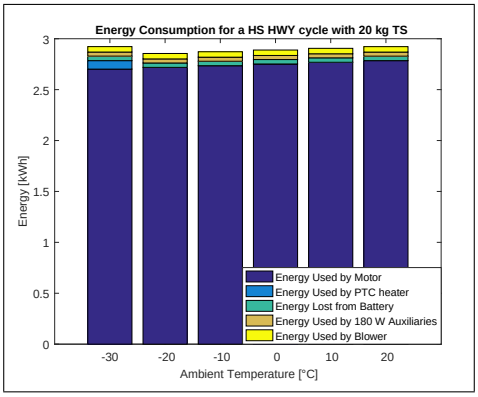

Figure 6.8: Energy breakdown for a HS HWY with 20 kg of TS at an initial coolant temperature of 60 degC.

storage case. Observed is the same slowly increasing traction energy as temperature increases due to the reduces motor/inverter efficiency at higher temperatures. In all but the -30 °C case, the heat energy is fully provided by the thermal storage. The same energy breakdown can be seen in quantitative form in Table 6.2.

Table 6.2: Energy break down for a HS HWY with 20 kg of TS at an initial coolant temperature of 60 °C.

	Energy Consumed by [kWh]				
Tamb [°C]	Traction	PTC Heat	Battery Losses	Auxiliary	Blower
-30	2.7016	0.0832	0.0444	0.0400	0.0533
-20	2.7185	0	0.0433	0.0400	0.0533
-10	2.7354	0	0.0434	0.0400	0.0533
0	2.7521	0	0.0435	0.0400	0.0533
10	2.7687	0	0.0437	0.0400	0.0533
20	2.7851	0	0.0438	0.0400	0.0533

At a thermal storage temperature of 80 °C, only 8 kg of ethylene-glycol/water

mixture is needed to meet the heating demand for the hot start highway cycle at all ambient temperatures. A consumption improvement from 207 Wh/km (baseline) to 175 Wh/km is observed at -30 °C ambient. The 0 kg of added storage case yields

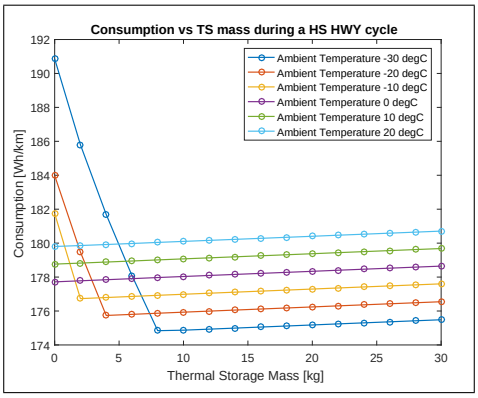

Figure 6.9: EV consumption vs. thermal storage size at varying ambient temperatures at an initial coolant temperature of 80 degC during a HS HWY cycle.

a consumption of 191 Wh/km. Therefore the consumption improvement is 8 % or 15 %. At 20 °C, the consumption increases by about 1 Wh/km with the added 30 kg of storage. This further strengthens the insignificance of added mass on the EV performance. Finally, Fig. 6.10 shows the heat provided by the PTC heater for an initial coolant temperature of 80 °C.

6.4 Thermal Storage Results - Hot Start Triple UDDS Cycle

The triple UDDS cycle was applied to the model to offer a comparison in a cycle which is just over 1 hour long. Similar trends are observed in this cycle, however it offers a more realistic cycle in terms of duration. As previously mentioned the cycle is 1 hour 9 minutes long, and is about 36 km in length. The thermal storage

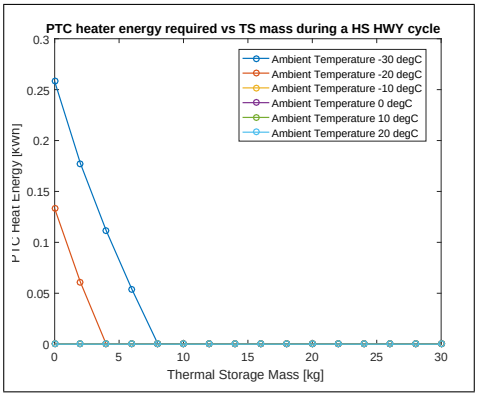

Figure 6.10: PTC heater load vs. thermal storage size at varying ambient temperatures at an initial coolant temperature of 80 degC during a HS HWY cycle.

mass range was changed to between 10 kg and 160 kg to accommodate the longer cycle. The dissimilarities between the different ambient temperature lines are a little more apparent in Fig. 6.11. Additionally, the -30 °C line appears to level off at a certain point, again due to the limited controls. A consumption improvement at this temperature was observed of between 13 % and 18 % with 160 kg of thermal storage. The heat energy supplied by the PTC heater for these simulations can be seen in Fig. 6.12. At 100 kg of 60 °C thermal storage, all but the two coldest ambient cases are

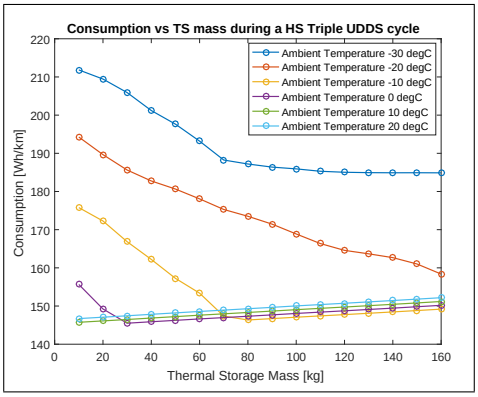

Figure 6.11: EV consumption vs. thermal storage size at varying ambient temperatures at an initial coolant temperature of 60 degC during a HS triple UDDS cycle.

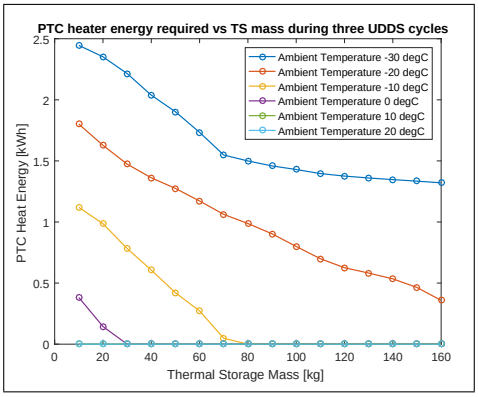

Figure 6.12: PTC heater load vs. thermal storage size at varying ambient temperatures at an initial coolant temperature of 60 degC during a HS triple UDDS cycle.

met. These results can be seen in Fig. 6.13 and Table 6.3. A 3.4 % reduction in traction energy is noticed when comparing the -30 °C and 20 °C cases.

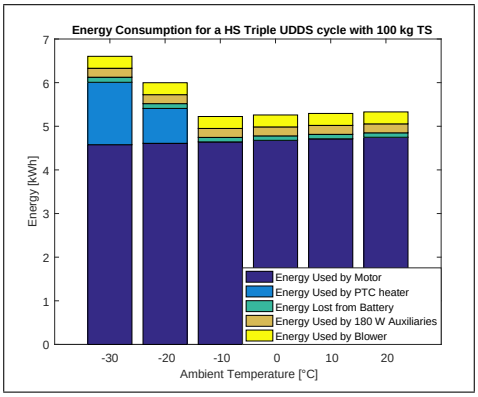

Figure 6.13: Energy breakdown for a HS triple UDDS with 100 kg of TS at an initial coolant temperature of 60 degC.

Table 6.3: Energy break down for a HS triple UDDS with 100 kg of TS at an initial coolant temperature of 60 °C.

	Energy Consumed by [kWh]				
Tamb [°C]	Traction	PTC Heat	Battery Losses	Auxiliary	Blower
-30	4.5779	1.4296	0.1168	0.2053	0.2738
-20	4.6095	0.7996	0.1100	0.2053	0.2738
-10	4.6425	0	0.1024	0.2053	0.2738
0	4.6777	0	0.1022	0.2053	0.2738
10	4.7128	0	0.1021	0.2053	0.2738
20	4.7479	0	0.1021	0.2053	0.2738

The 80 °C thermal storage shows the most promise. It has the most energy, and since the effect of the losses and mass are almost negligible, the hottest, heaviest storage has the best results. The most promising mass for the triple UDDS cycle at -30 °C is at 120 kg, where the minimum potential consumption is achieved. This can be extracted from Fig. 6.14 and Fig. 6.15. The improvement in consumption for the -30 °C case is between 29 % and 36 %. This decrease in consumption is made possible by the fact that the thermal storage provides all of the heating necessary for passenger comfort. In the HS triple UDDS baseline, the energy required to heat the vehicle at -30 °C was 2.85 kWh. To put this in perspective, the TS storage was used to displace an energy consumption of 15 % of the total vehicle usable battery energy (19.2 kWh).

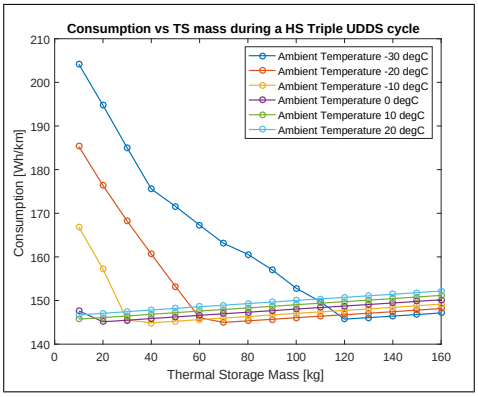

Figure 6.14: EV consumption vs. thermal storage size at varying ambient temperatures at an initial coolant temperature of 80 °C during a HS triple UDDS cycle.

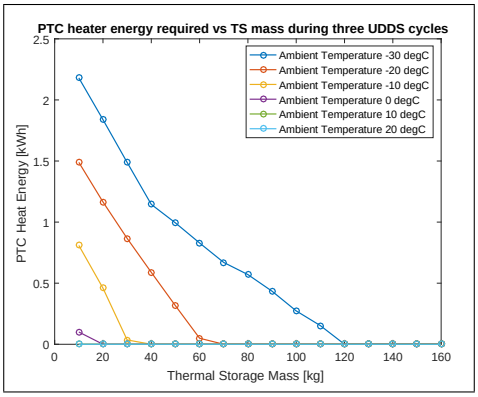

Figure 6.15: PTC heater load vs. thermal storage size at varying ambient temperatures at an initial coolant temperature of 80 °C during a HS triple UDDS cycle.

6.5 Available Energy

As previously mentioned in Chapter 2, the amount of energy in a thermal storage is proportional the change in storage temperature. Depending on the ambient temperature, the available energy in the thermal storage can vary. Since at lower temperatures, the heat losses from the cabin are higher, the coolant temperature must be higher to sustain this increased demand. Therefore, the coolant ΔT is lower and thus

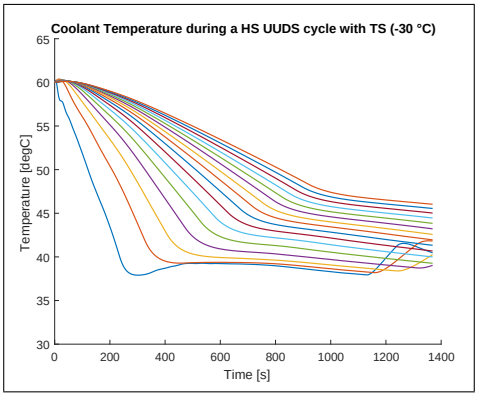

Figure 6.16: Coolant temperature for a HS UDDS at -30 °C, with TS masses varying from 0 kg (the lowest line) to 30 kg (the highest line) at increments of 2 kg.

the usable energy in the storage is lower as well. This difference is observed when comparing the -30 °C case of Fig. 6.16 to the -10 °C case of Fig. 6.17. In the -30

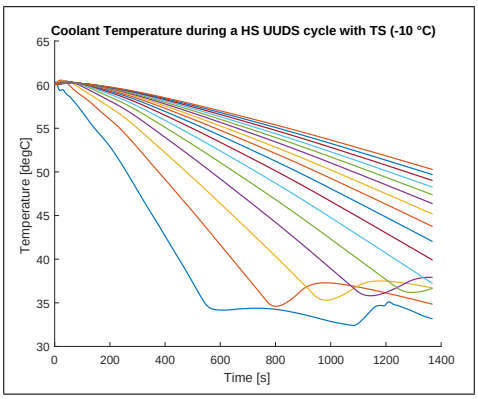

Figure 6.17: Coolant temperature for a HS UDDS at -10 °C, with TS masses varying from 0 kg (the lowest line) to 30 kg (the highest line) at increments of 2 kg.

°C case, the highest ΔT is about 22 °C compared to 26 °C in the -10 °C case. For the same mass, this would yield an increase of 18 % usable energy. Table 6.4 displays some theoretical energy values for various tanks. The ΔT of 20 is an approximation for the 60 °C initial coolant temperature, while the ΔT of 40 represents the 80 °C cases. Based on these calculations, an 80 kg storage should suffice for meeting

the needs of the triple cycle at -30 °C, as compared to the simulated 120 kg result. Chapter 7, will provide some clearance as to the reason for this discrepancy.

Table 6.4: Thermal storage tank energy based on some masses and ΔT values.

Mass [kg]	ΔT [°C]	Energy in Tank [kWh]
2	20	0.037
2	40	0.073
30	20	0.55
30	40	1.10
80	20	1.47
80	40	2.93
160	20	2.93
160	40	5.87

Chapter 7

Modified Controller for Improved Results, Vehicle Charging Implications and the Impact of the TS System on Range and Yearly Consumption

7.1 New Controller and Updated Results

A trend that was observed during the analysis of the thermal storage simulations was that at low temperatures (-30 °C and -20 °C), the slope of the decrease in consumption would begin to decrease after a certain amount of TS was added. Adding more thermal storage, was having a less significant impact. The controller was blamed for

this and it was concluded that even with a sub-optimal controller, the benefits of the TS were significant. A deeper look into this result was taken and is presented in this section. Fig. 7.1 shows the coolant temperature profiles for -30 °C ambient with varying TS masses during a HS UDDS cycle. The most rapidly decreasing coolant temperature line (the lowest one) in this plot is the 0 kg of added TS mass case, increasing by 2 kg per line all the way up to the 30 kg highest line. The most important feature to notice from this graph is the cornering temperature where the PTC heater comes online. This occurs at different times during the simulation since

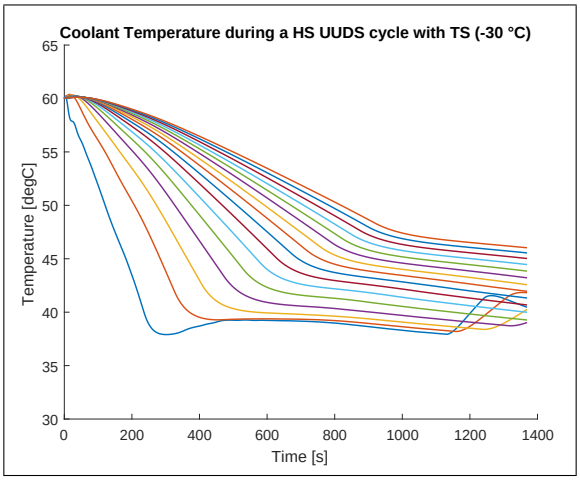

Figure 7.1: Coolant temperature for a HS UDDS cycle at -30 °C, with TS masses varying from 0 kg (the lowest line) to 30 kg (the highest line) at increments of 2 kg showing the varying datum temperatures.

the bigger thermal storage will conserve have more energy. The corner also seems to occur at different temperatures. Considering that the energy in a thermal storage is directly proportional to the change in temperature, this is a serious concern. With the original controller, it seems that the benefit of adding more thermal storage is only partially captured due to the reduction in temperature change. The bigger tanks are cornering at higher temperatures thus providing less energy. The shortcomings

of the controller can be seen in Fig. 7.2 where some data from a HS UDDS cycle at -30 °C with 30 kg of storage is presented. As previously discussed in Chapter 5, the heater comes online at 80 % valve control, as it is design to do. However, the heater provides enough energy to significantly slow the valve control signal down, forcing it to never to reach 100 %. This indicates the the heat exchanger is not operating to its full capability and therefore the coolant temperature must stay higher. This means the PTC heater must stay on at a higher level, and for longer in some cases. With this control strategy, the cabin temperatures for various cycles can be seen in Fig. 7.3. From this plot we can see that the temperatures hardly deviate from 20 °C, with the exception of the initial drop, and from this it was determined that the controller was adamant. However when considering the above discussion about the energy storage, it was determine that the controller was indeed suboptimal and as a result was modified.

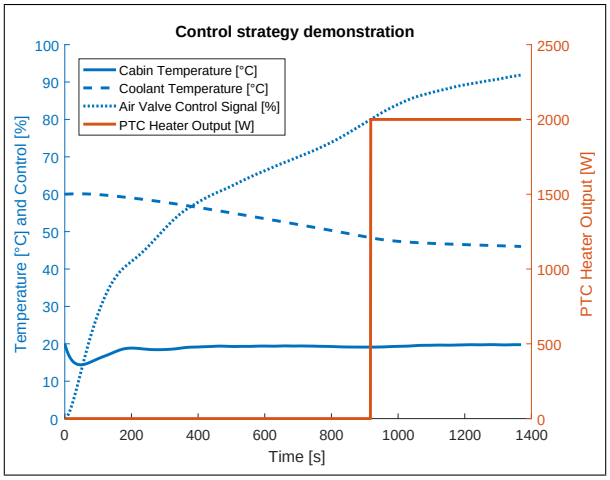

Figure 7.2: Plot of the control signal, PTC heater output, cabin temperature and coolant temperature for a HS UDDS cycle with 30 kg TS to show control shortcomings.

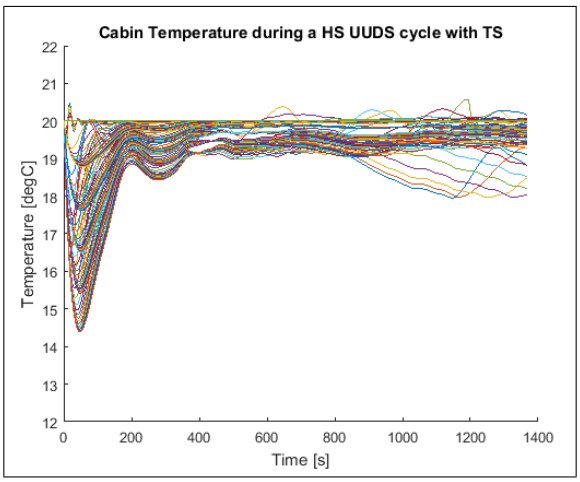

Figure 7.3: Cabin temperature for all temperatures and masses during a HS UDDS with TS.

The new controller simply adjusted the PTC activation command from the "air valve 80 % open" to "air valve 100 % open". This would ensure that as much of the TS energy as possible was used in all cases before the PTC heater was engaged. The new control scheme is depicted in Fig. 7.4. From this plot, it can be seen that the

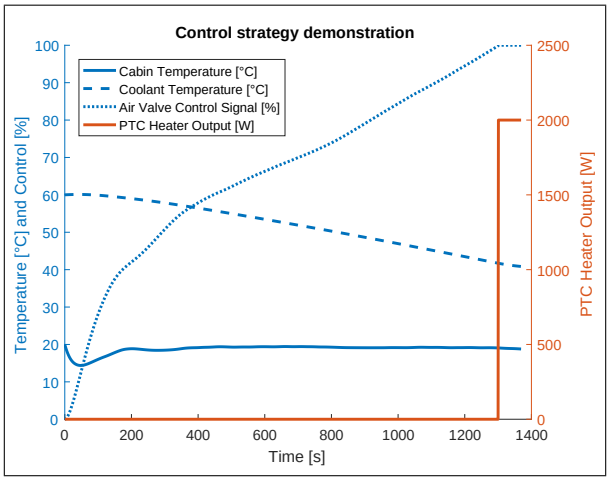

Figure 7.4: Plot of the control signal, PTC heater output, cabin temperature and coolant temperature for a HS UDDS cycle with 30 kg TS to show new control benefits.

PTC heater now only turns on when the valve is diverting 100 % of the air to the

heat exchanger. This allows the coolant temperature to further drop, saving precious battery energy and decreasing the consumption. Additionally, from 7.4 it appears to have minimal impact to the cabin temperature for this 30 kg, -30 °C ambient case. However, looking at Fig. 7.5, which displays all temperatures and masses, a more noticeable deviation in the cabin temperature is observed in some cases. This fluctuation is attributed to the coolant temperature decreasing past the minimum requirement and that when the PTC heater finally comes on, it is slow to warm the coolant back up. The coolant temperature results for the new controller can be seen in Fig. 7.6. With the updated controller, the coolant temperatures are cornering at much closer temperatures indicated a fairer comparison of the TS mass.

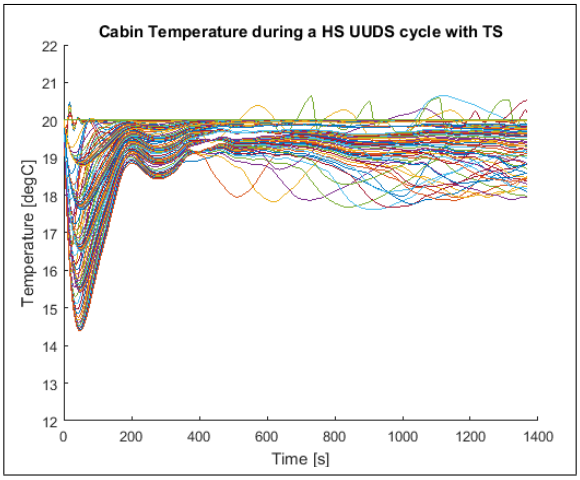

Figure 7.5: Cabin temperature for all temperatures and masses during a HS UDDS with TS with the modified controller.

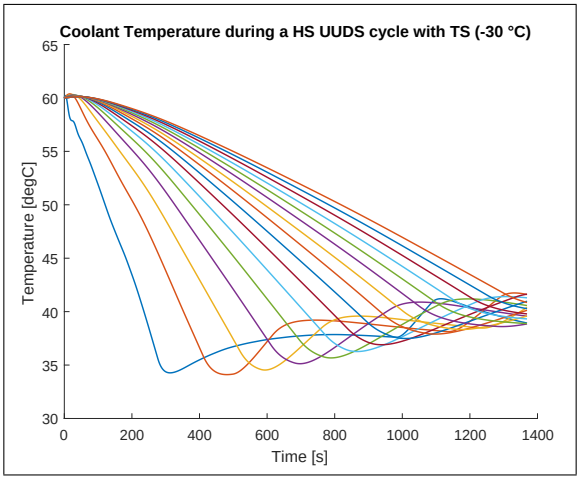

Figure 7.6: Coolant temperature for a HS UDDS cycle at -30 °C, with TS masses varying from 0 kg (the left-most line) to 30 kg (the right-most line) at increments of 2 kg with the modified controller.

The resulting consumption implications of the modified controller can be seen in Fig. 7.7. When compared to Fig. 6.1, the -30 °C shows much better results. Instead of requiring an extrapolated 60 kg of TS mass to meet all of the heating needs, with the new controller, only about 30 kg are required. This control strategy gives a much more accurate view of the impact of thermal storage at low ambient temperatures.

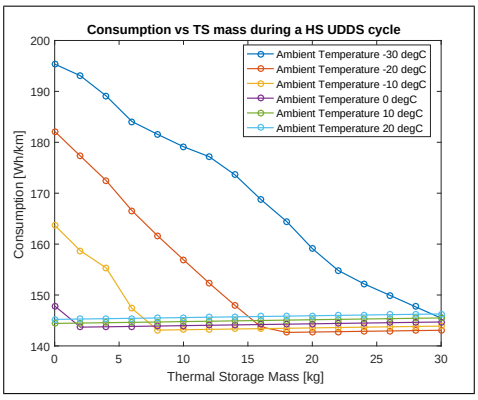

Figure 7.7: EV consumption vs. thermal storage size at varying ambient temperatures at an initial coolant temperature of 60 °C during a HS UDDS cycle with modified controller.

Similarly, the triple UDDS cycle was simulated at an initial coolant temperature of 80 °C with the modified controller. The updated consumption results are plotted in Fig. 7.8. From this plot it is observed that with the new controller only 80 kg of TS is required to meet all hearting requirements for this cycle as compared to 120 kg with the original controller seen in Fig. 6.14. Some further optimization of the controller is required as the consumption appears to slow in the 60 °C cases. However, a significant improvement was noticed. Due to time constraints, the remaining TS simulations were not performed and therefore the results are not included in this report.

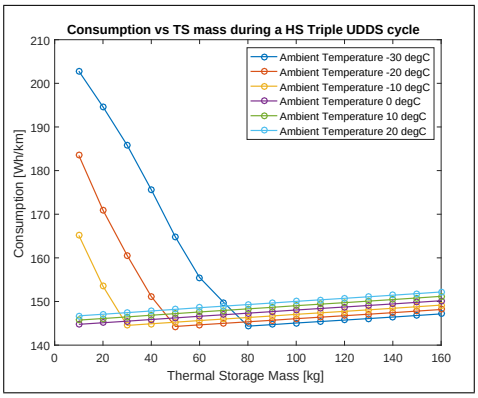

Figure 7.8: EV consumption vs. thermal storage size at varying ambient temperatures at an initial coolant temperature of 80 °C during a HS triple UDDS cycle with modified controller.

7.2 Vehicle Charging Time

Another consideration of having this system installed on an electric vehicle is the increased charging time. The primary discussions thus far have been regarding consumption improvement. However, similarly important is the impact on the charging time. The largest thermal storage examined in this research was a 160 kg tank with

a ΔT of 110 °C (-30 °C to 80 °C). Using a specific heat of 3.3 kJ/kg K, the total energy required to heat this storage is 16.1 kWh. Additionally, the 150 watt coolant pump is required to be run for the duration of the heating process and an assumed average 100 watts of losses from the tank during charging. This could add as much as 2 kWh to energy requirement for an 8 hour charging time. The Nissan Leaf sized battery pack has about 19.2 kWh of usable energy and it is assumed that a 6.6 kw charger is on board [46].

A level 1 charger is a standard household outlet with 120 volts and a maximum of 15 amps [47]. This charger can output a maximum power of 1.8 kW. With this charger, the 19.2 kWh battery pack could undergo a full charge in 10.7 hours. With the addition of the thermal storage and losses, the charge time for the vehicle is increased to 22.8 hours. Halving the mass to 80 kg, the charge time is reduced to 17.6 hours. With a level 2 charger, a 240 volt, 30 amp supply is available. The maximum draw from a level 2 charger is 7.2 kw. Therefore the on-board, 6.6 kW charger is the limiting factor. With this 6.6 kW charger the battery alone could be charged in 2.9 hours. The charging of the 160 kg tank adds roughly 2.3 hours for a full charge time of 5.2 hours. With the level 2 charger, since the process takes much less time, the impact of the pump and heat losses is relatively reduced. With an 80 kg tank, the charging time is reduced to 4.3 hours. Regardless of the level of charging, the impact of heating a large tank on the charging time is significant. However, with a level 2 charger, the vehicle can still be fully charged overnight or during work hours.

7.3 Range of an Electric Vehicle with Thermal Storage

The range calculated for the baseline model was done by taking the ratio of total SOC to the SOC used during the cycle and multiplying this by the distance travelled. This assumed that the identical cycle was driven over and over again with the same initial conditions until battery depletion. Since running simulations until the battery was depleted was unrealistic due to time constraints, the SOC ratio was used to extrapolate and estimate the range. For the baseline model, this estimation was realistic, since the initial conditions were repeatable as SOC dropped. However, in the case of the TS model, the initial condition of a hot TS could not be achieved with out plugging the vehicle in and re-warming it. After a given cycle, the TS would either have completely depleted or would have some amount of energy left. If all of the heating requirements were met during that cycle, the same could not be assumed for a following cycle. A prediction of when the thermal storage was fully depleted, was required. This was done by assuming a different datum temperature of the coolant for each ambient temperature, and extrapolating based on how much the coolant temperature had dropped within the first cycle. Consumption before the coolant temperature reached datum was assumed to be equal to that of the first TS cycle and consumption thereafter was assumed to be that of the HS baseline case for the same cycle. The results of these calculations were plotted in Fig. 7.9 for the triple UDDS cycle with an initial coolant of 80 °C and using the updated controller. From this plot it can be observed that even with 160 kg of TS mass, the heating demand for the maximum range cannot be met. Since 160 kg (roughly 160 L) is already an

unrealistic size, the selected mass would have to be one which offers the most benefit based on average temperatures, driving styles and driving distances.

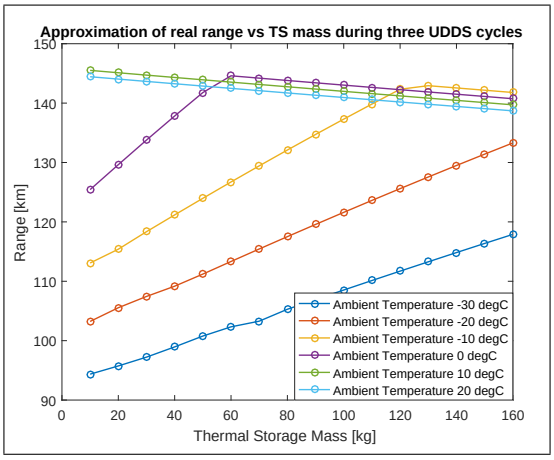

Figure 7.9: EV range vs. thermal storage size at varying ambient temperatures at an initial coolant temperature of 80 °C during a HS triple UDDS cycle with modified controller.

7.4 Optimal Thermal Storage Mass and Battery Equivalent for Minimizing Yearly Consumption based on the Triple UDDS Cycle and an Ottawa, Canada Climate

After acquiring an understanding of how different TS masses impacted the consumption at various temperatures, the question of "Which mass to choose?" arose. The impact of the thermal storage at low ambient temperatures is significantly positive however, at warmer temperatures, the additional mass has a negative impact on vehicle consumption. The best selection of mass is dependant on several factors including,

TS initial temperature, yearly climate, drive cycle (urban or highway), and driving distance. Since the 80 °C initial coolant temperature showed the most promise, this will be the assumed initial coolant temperature for this section of the analysis. The triple UDDS cycle simulates a 36 km drive, and much of the data collected was using this cycle. From, [48], it can be extracted that roughly 90 % of all trips made in the U.S. were less than 36 km. The plot used for this extraction can be seen in Appendix H. Since the Canadian equivalent of the data was not available, it was assumed that the Ottawa daily driving would be similar to that found in [48]. It was then assumed that the triple UDDS could be used as an accurate representation, as it is at least as long as 90 % of trips made in the U.S. (and assumed Ottawa). It was also taken from the daily average temperature in Ottawa in [49], that roughly 4 months of the year were greater than 15 °C, 2.5 month of the year were between 5 °C and 15 °C, 3.5 months of the year were between -5 °C and 5 °C, and 2 months of the year were around -10 °C. At temperatures above 15 °C, no heating is necessary and the data from 20 °C was assumed to be an accurate representation for this temperature range. The data from the -10 °C, 0 °C, 10 °C and 20 °C simulations was used to represent the "-10 °C", "-5 °C to 5 °C", "5 °C to 15 °C", and the "greater than 15 °C" temperature ranges respectively. The temperature plot used from [49] can also be seen in Appendix H.

The weighted average of the baseline line HS triple UDDS consumption was determined to be 170 Wh/km, based on the product of the time spent at various temperatures and the consumption at that temperature. The same weighted average was taken for the TS system at each different mass. The result is plotted in Fig. 7.10 along with the reference 170 Wh/km line. The optimal TS mass based on the above

assumptions appears to be 30 kg. Assuming that every trip began with a hot TS, was shorter than the triple UDDS, and had similar cycle characteristics, the average yearly energy savings would be about 20 Wh/km or 12 %. It is interesting to note that even though the simulation results from -20 °C and -30 °C were unused in this analysis, any TS mass (including 160 kg) has a positive impact on the average yearly consumption.

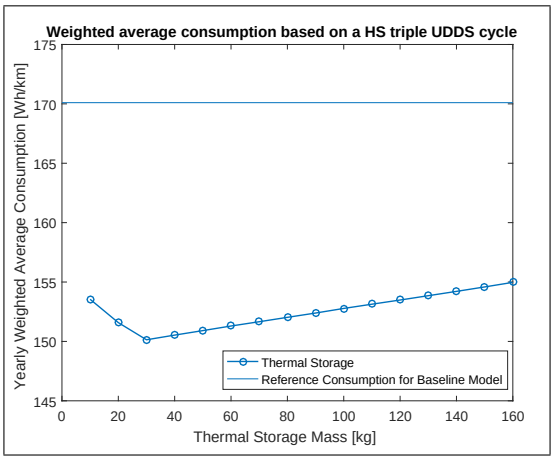

Figure 7.10: Average annual weighted consumption vs. thermal storage size at an initial TS temperature of 80 °C during a HS triple UDDS cycle.

30 kg of 50/50 ethylene-glycol/water mixture TS at 80 °C with an average datum temperature of 30 °C possesses about 1.375 kWh of energy. Assuming no major modification to the coolant system, the cost of the TS system would include an insulated tank, some additional pipe and fitting, and 30 kg of coolant. It is difficult to price exactly however, it is assumed that this system would cost less than $ 100. From [46], an equivalent Nissan Leaf Li-ion battery, with an 80 % maximum depth of discharge would cost $ 516 and have a mass of 12.3 kg. While this battery pack may be lighter, it would cost significantly more and would simply increase the vehicle range year-round instead of targeting the fluctuation problem.

Chapter 8

Conclusions and Future Work

8.1 Conclusion

It has been shown through simulation that an electric vehicle can have its range reduced by over 50 % in cold driving conditions as compared to mild conditions. In areas where ambient temperature fluctuates significantly throughout the year, the range of an electric vehicle can vary significantly. The range reduction at cold temperatures is largely due to the increased electrical load from the electrical heater used for passenger thermal comfort. A thermal storage based system has been presented and modelled in this thesis which aims to improve range in electric vehicles at low ambient temperatures by offsetting the a portion of the cabin heating demand. In this system, the storage is heated off-line using grid energy (in parallel with battery charging). Once heated, the storage has enough energy to meet all or a portion of the heating energy required, depending on storage size and planned drive cycle.

First, a baseline simulation model was created in AMESim. This model was a representative model of the Nissan Leaf to an accuracy of less than 4 %. The baseline

simulations showed that during a cold start drive cycle, the range at -30 °C was reduced as much as 63 % compared to the 20 °C case. The simulations also showed that with a preconditioned vehicle, the range reduction was attenuated to a 38 % range reduction. This indicated a range improvement of more than 25 % strictly due to preconditioning.

The thermal storage model was then built in AMESim and simulated. These simulations showed that with an 80 kg, 80 °C thermal storage tank, all the thermal needs of a 1 hour and 9 minute city cycle could be provided thus improving the calculated consumption by 36 % and possessing the same consumption as in the 20 °C. Based on this cycle, the estimated range can be improved by 30 % in temperatures below 0 °C. With an The charging implications of such a tank were shown to be significant however, with a level 2 charger, the charging time is less than 6 hours. The losses on the tank were not considered in the model though with proper insulation, were shown to be less than 10 % of the heat delivered to the cabin. Additionally, the range reduction due to the increase in vehicle mass was determined to be minor.

Based on an Ottawa, Canada climate, and the triple UDDS cycle with 80 °C thermal storage, it was determined that 30 kg was the optimal amount of thermal storage mass. Additionally, it was determined that an electric battery with equivalent capacity would cost $ 516 compared to less than $ 100 for the TS system. Based on the simulations presented in the thesis, thermal storage could offer significant relief to the drastic reduction in electric vehicle range in cold weather, though experimental validation is still required.

8.2 Future Work

Due to time constraints, not everything could be considered. This section will offer some thoughts as to what future work could be performed following this research. Aside from completing the simulations with the modified controller, and further optimizing the controller, here are some interesting future work ideas.

An assumption made throughout this research was that the cabin temperature was to be kept at 20 °C in order to achieve passenger thermal comfort. However, with techniques mentioned such as heated seats and a steering wheel, a lower cabin temperature may suffice. It is difficult to quantify thermal comfort since so many factors including passenger initial thermal comfort level, passenger thermal preferences, passenger clothing, passenger size, solar irradiance, etc. can affect the thermal comfort of a person in a vehicle. An analysis on the range/consumption implications of reducing the desired (or set) cabin temperature could be performed to assess potential improvements.

Another future consideration would stem from the fact that a vehicle can initially have a cold cabin and battery with a warm thermal storage. The transient heat loss calculations have showed that a situation where a vehicle ends a drive with warm coolant, could then begin its next trip with a warm TS tank but is other wise cold. Some simulations to show the ramifications of these initial conditions could be performed and analyzed.

Alterations to the thermal storage system itself could also be done. For example adding a heat pump to the system. This would combine the high heat pump efficiency at moderate temperatures and have the thermal storage provide additional heat in extreme cold conditions. Furthermore, different thermal storage materials could be

used, such as PCM.

At cold temperatures, regenerative is sometimes not possible or extremely inefficient. In other scenarios, the breaking is so severe, that the regenerated current is too high for the battery to accept. It could however be possible to store this surplus regenerative breaking energy in the thermal storage through the PTC heater. This is another investigation area which could merit some attention.

Any of these ideas have the potential to further increase the range in cold climate. This could in turn further increase the appeal of electric vehicles, aiding in the global reduction of carbon emissions.

Appendix

A AMESim Model Parameters

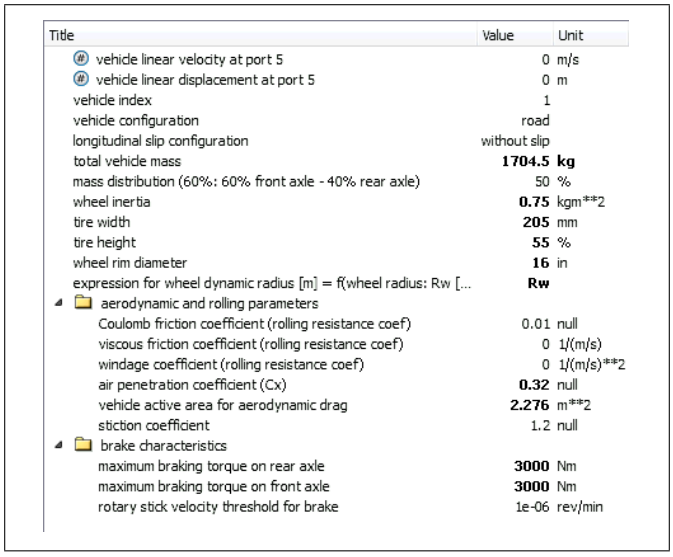

Title	Value	Unit
vehicle linear velocity at port 5	0	m/s
vehicle linear displacement at port 5	0	m
vehicle index	1	
vehicle configuration	road	
longitudinal slip configuration	without slip	
total vehicle mass	**1704.5**	**kg**
mass distribution (60%: 60% front axle - 40% rear axle)	50	%
wheel inertia	**0.75**	kgm**2
tire width	**205**	mm
tire height	**55**	%
wheel rim diameter	**16**	in
expression for wheel dynamic radius [m] = f(wheel radius: Rw [...	**Rw**	
aerodynamic and rolling parameters		
Coulomb friction coefficient (rolling resistance coef)	0.01	null
viscous friction coefficient (rolling resistance coef)	0	1/(m/s)
windage coefficient (rolling resistance coef)	0	1/(m/s)**2
air penetration coefficient (Cx)	**0.32**	null
vehicle active area for aerodynamic drag	**2.276**	m**2
stiction coefficient	1.2	null
brake characteristics		
maximum braking torque on rear axle	**3000**	Nm
maximum braking torque on front axle	**3000**	Nm
rotary stick velocity threshold for brake	1e-06	rev/min

Figure 1: AMESim vehicle block parameters.

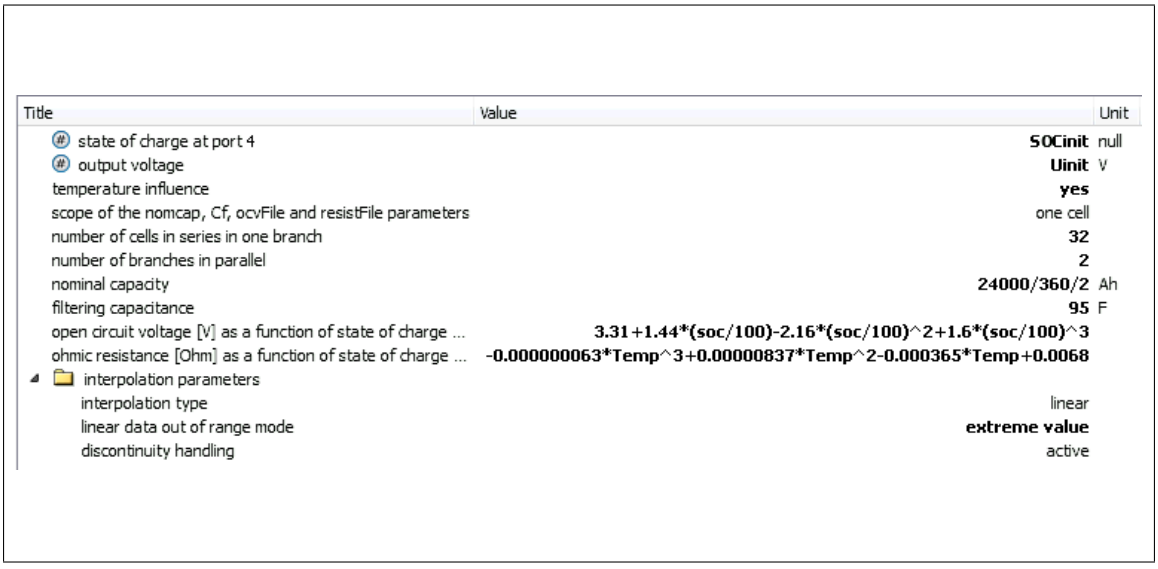

Title	Value	Unit
state of charge at port 4	**SOCinit**	null
output voltage	**Uinit**	V
temperature influence	**yes**	
scope of the nomcap, Cf, ocvFile and resistFile parameters	one cell	
number of cells in series in one branch	**32**	
number of branches in parallel	**2**	
nominal capacity	**24000/360/2**	Ah
filtering capacitance	**95**	F
open circuit voltage [V] as a function of state of charge ...	**3.31+1.44*(soc/100)-2.16*(soc/100)^2+1.6*(soc/100)^3**	
ohmic resistance [Ohm] as a function of state of charge ...	**-0.000000063*Temp^3+0.00000837*Temp^2-0.000365*Temp+0.0068**	
interpolation parameters		
interpolation type	linear	
linear data out of range mode	**extreme value**	
discontinuity handling	active	

Figure 2: AMESim high voltage battery block parameters.

Title	Value	Unit
peak power level 1	1000	W
peak power level 2	1000	W
peak power level 3	1000	W
peak power level 4	1000	W
peak power level 5	2000	W
nominal power level 1	1000	W
nominal power level 2	1000	W
nominal power level 3	1000	W
nominal power level 4	1000	W
nominal power level 5	2000	W
peak length level 1	1500	s
peak length level 2	1500	s
peak length level 3	1500	s
peak length level 4	1500	s
peak length level 5	1500	s
reference temperature	20	degC
corrective coefficient alpha	0	null
minimum voltage	0.1	V
efficiency	0	null

Figure 3: AMESim PTC heater block parameters.

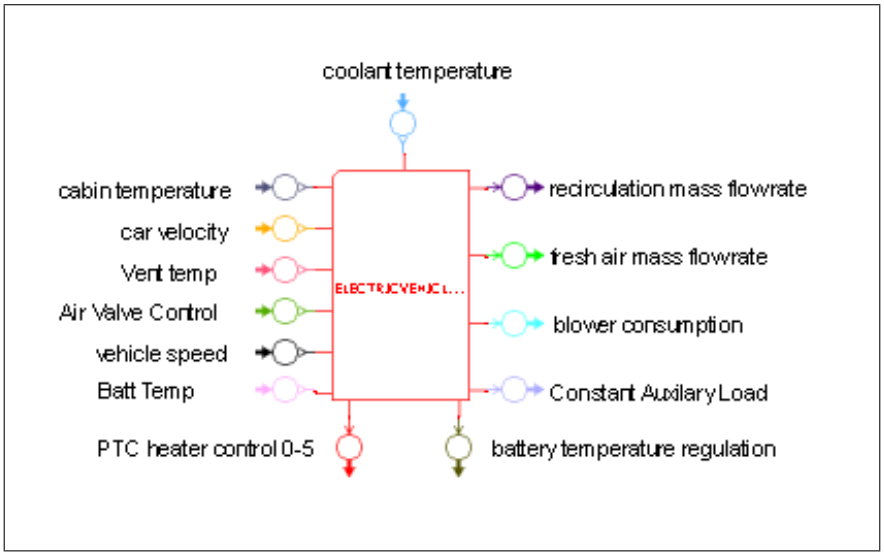

Figure 4: AMESim controller supercomponent showing port numbers.

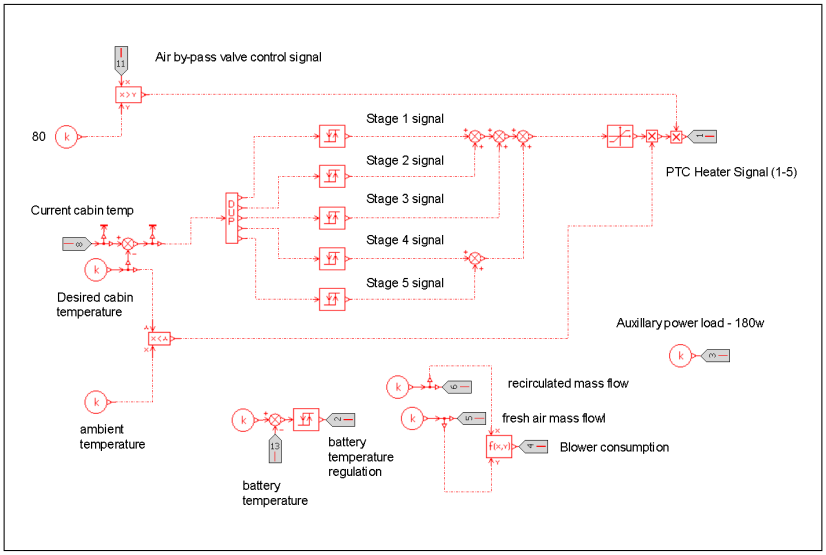

Figure 5: Model HVAC controller layout.

B The Argonne Comparison

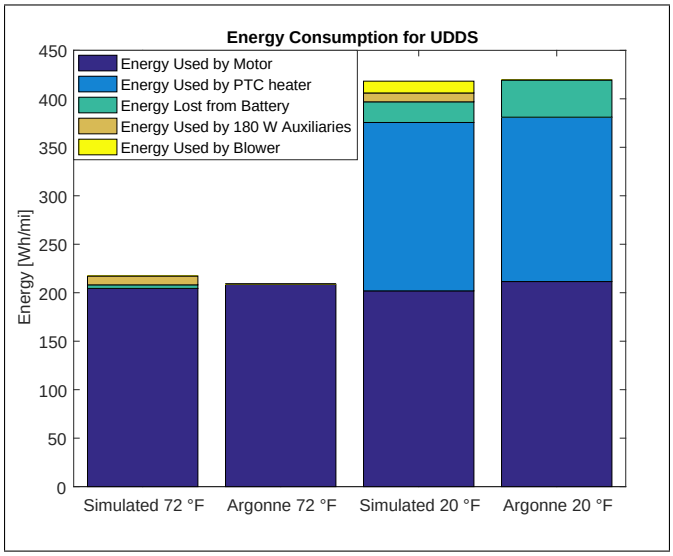

Figure 6: Simulated energy consumption in Wh/mi during a cold start UDDS at -7 degC (20 deg F) and 22 degC (72 degF).

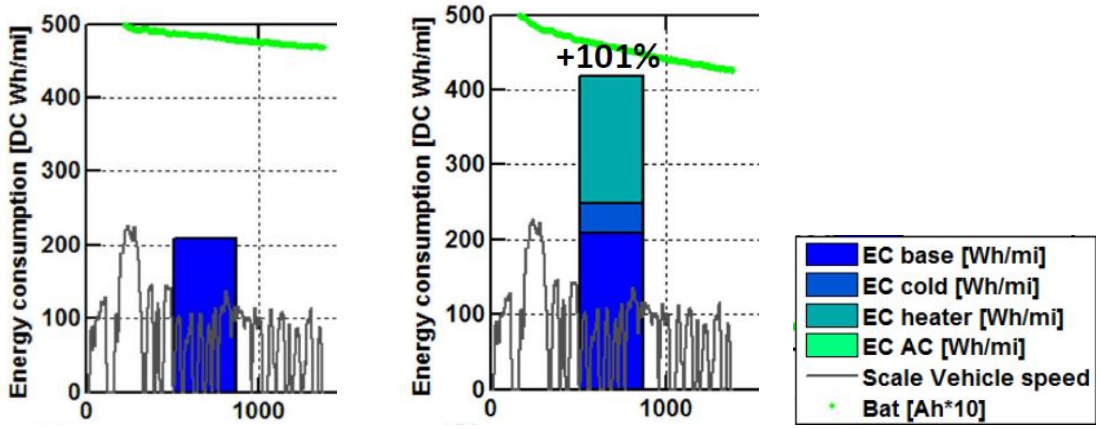

(a) 22 degC (72 degF). (b) -7 degC (20 deg F). (c) Legend.

Figure 7: Experimental energy consumption during the UDDS from [6].

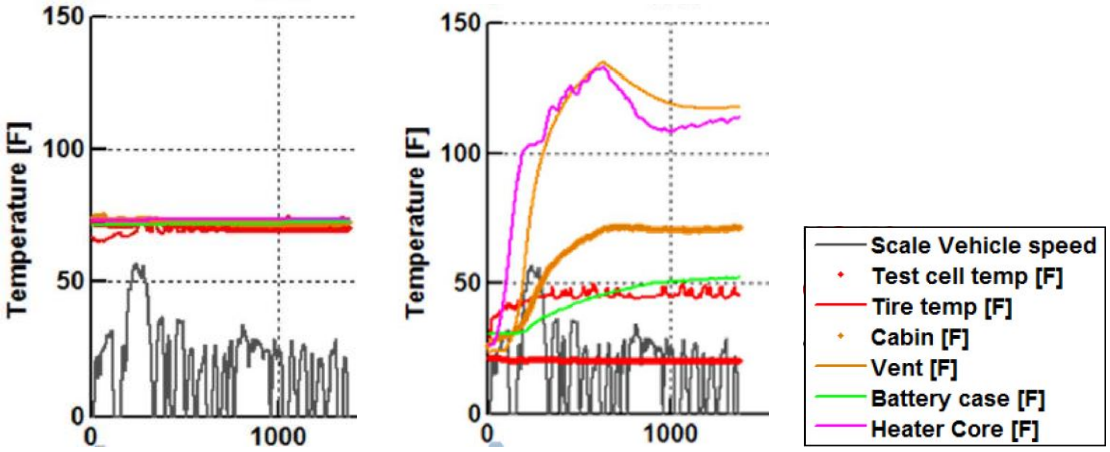

(a) 22 degC (72 degF). (b) -7 degC (20 deg F). (c) Legend.

Figure 8: Experimental temperature distribution during the UDDS from [6].

C Cold Start HWY Drive Cycle Results for the Baseline Model

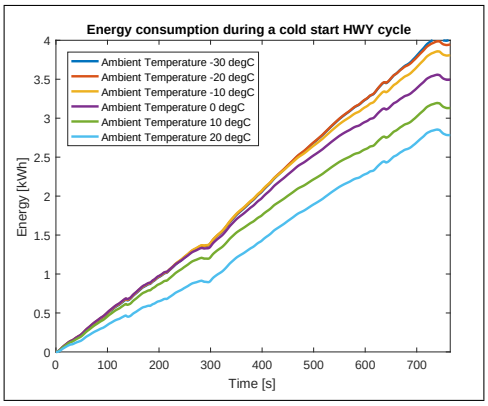

Figure 9: Simulated cumulative energy consumption in kWh during a CS HWY cycle.

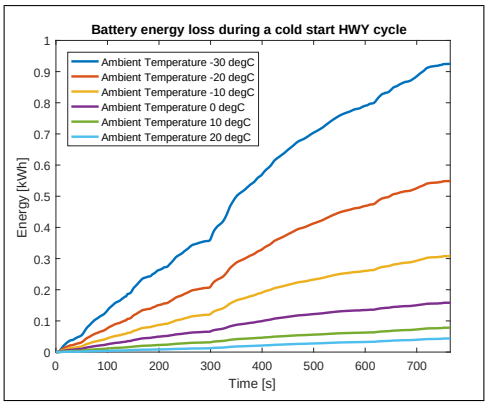

Figure 10: Simulated cumulative energy loss in kWh during a CS HWY cycle.

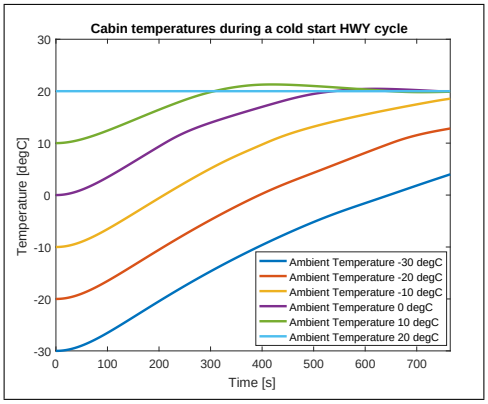

Figure 11: Cabin temperature during a CS HWY cycle.

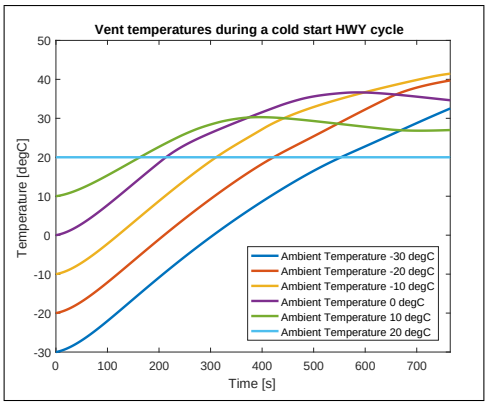

Figure 12: Vent temperature during a CS HWY cycle.

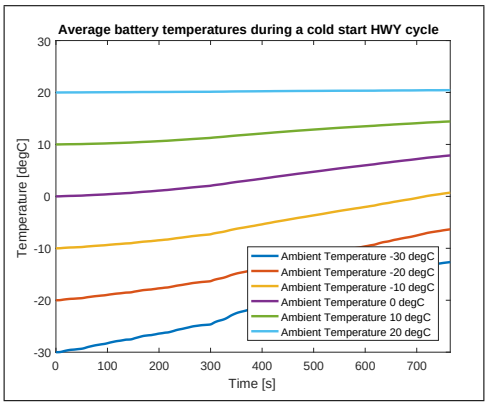

Figure 13: Average battery temperature during a CS HWY cycle.

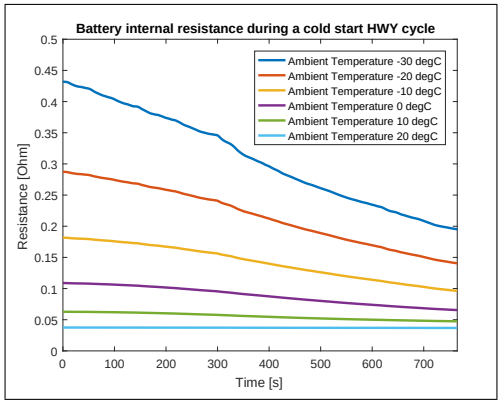

Figure 14: Battery internal resistance during a CS HWY cycle for one module.

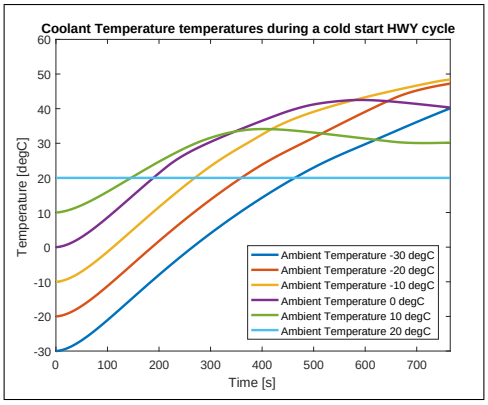

Figure 15: Coolant temperature during a CS HWY cycle.

D Cold Start Triple UDDS Drive Cycle Results for the Baseline Model

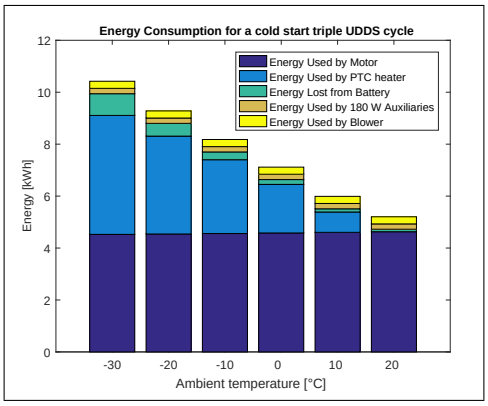

Figure 16: Simulated energy consumption in kWh during three UDDS cycles.

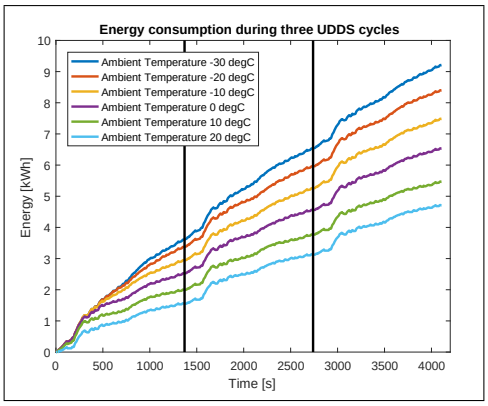

Figure 17: Simulated cumulative energy consumption in kWh during three UDDS cycles.

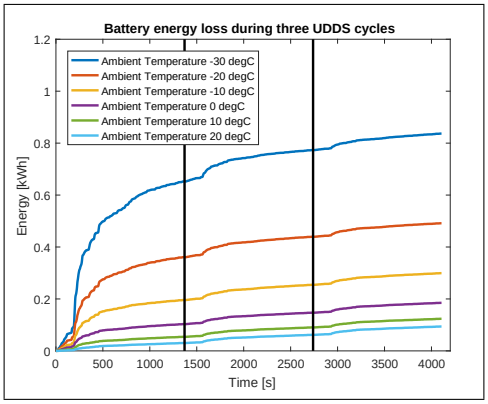

Figure 18: Simulated cumulative energy loss in kWh during three UDDS cycles.

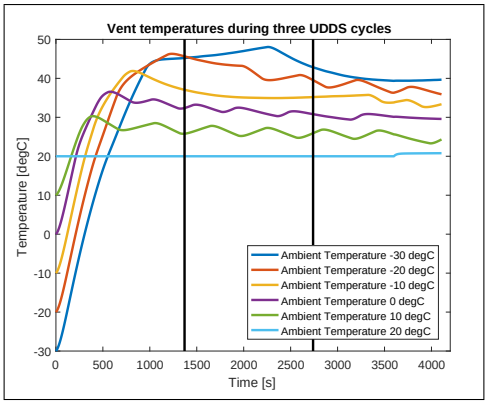

Figure 19: Vent temperature during three UDDS cycles.

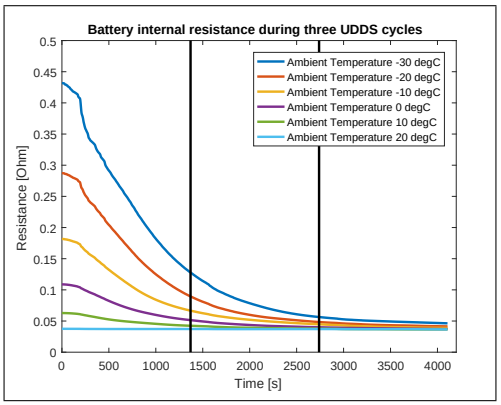

Figure 20: Battery internal resistance during three UDDS cycles for one module.

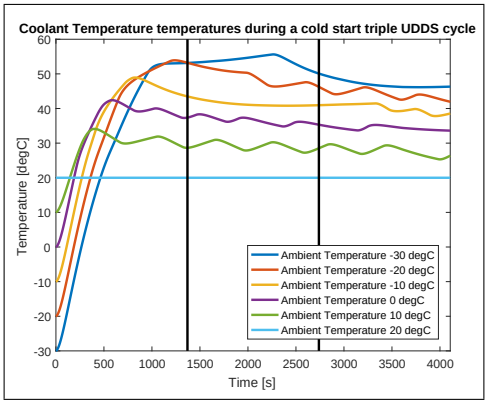

Figure 21: Coolant temperature during three UDDS cycles.

E Hot Start Triple UDDS Drive Cycle Results for the Baseline Model

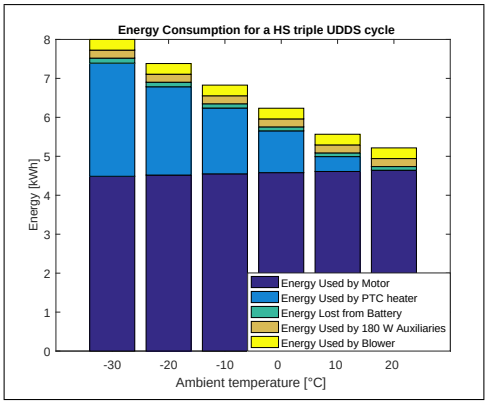

Figure 22: Simulated energy consumption in kWh during a HS triple UDDS cycles.

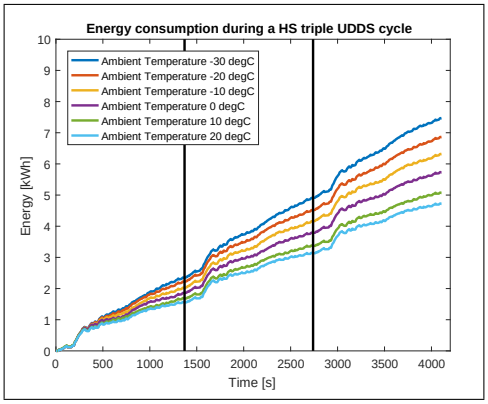

Figure 23: Simulated cumulative energy consumption in kWh during a HS triple UDDS cycles.

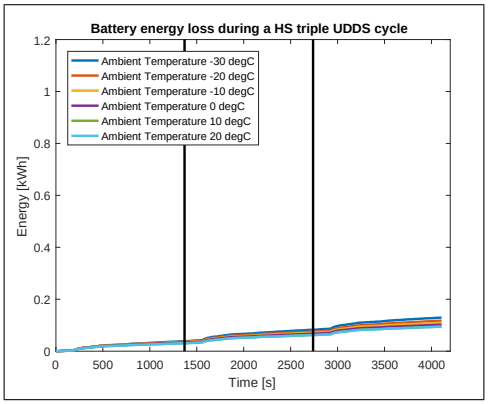

Figure 24: Simulated cumulative energy loss in kWh during a HS triple UDDS cycles.

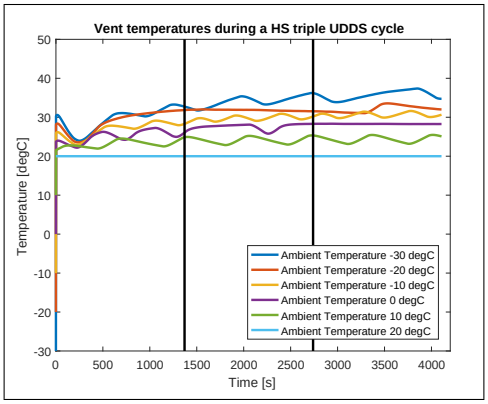

Figure 25: Vent temperature during a HS triple UDDS cycles.

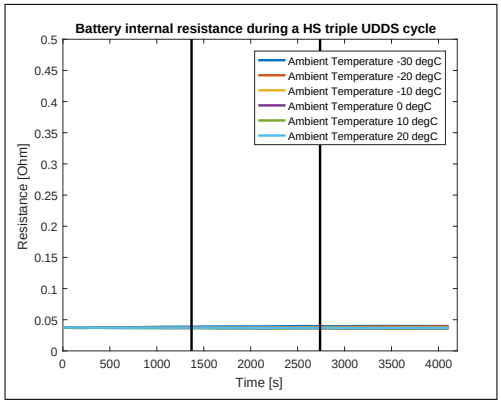

Figure 26: Battery internal resistance during a HS triple UDDS cycles for one module.

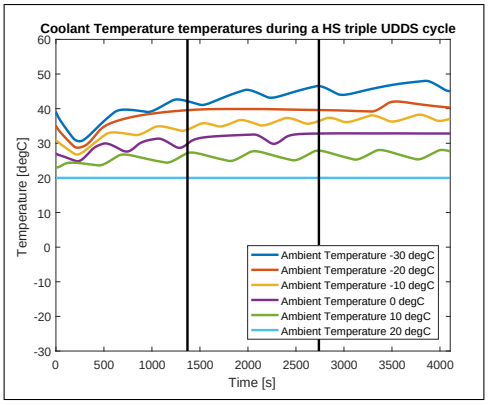

Figure 27: Coolant temperature during a HS triple UDDS cycles.

F Hot Start UDDS Drive Cycle Results for the Baseline Model

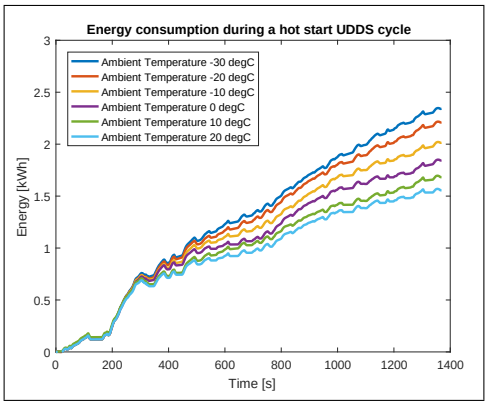

Figure 28: Simulated cumulative energy consumption in kWh during a HS UDDS cycle.

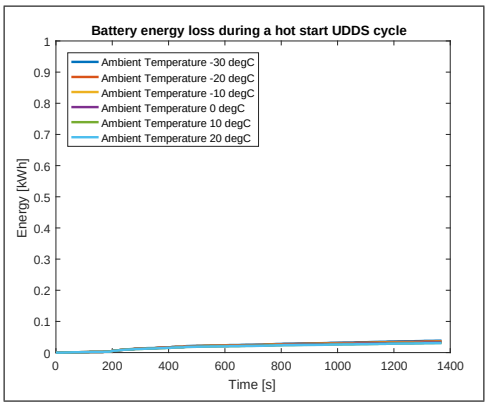

Figure 29: Simulated cumulative energy loss in kWh during a HS UDDS cycle.

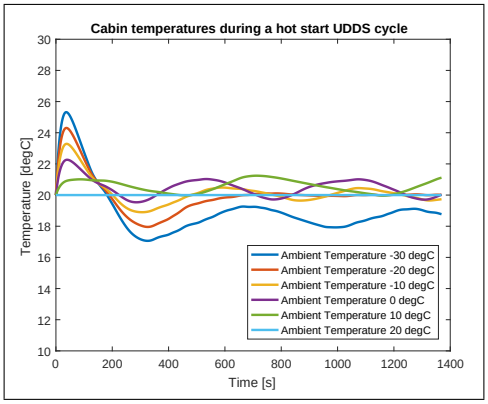

Figure 30: Cabin temperature during a HS UDDS cycle.

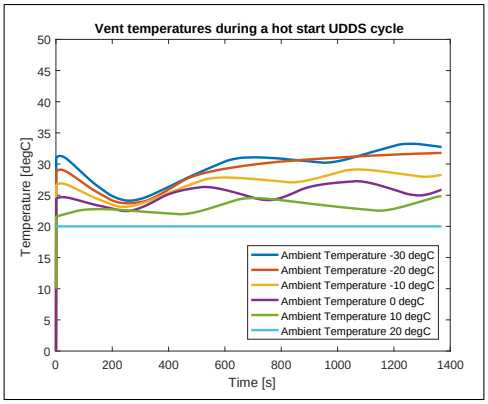

Figure 31: Vent temperature during a HS UDDS cycle.

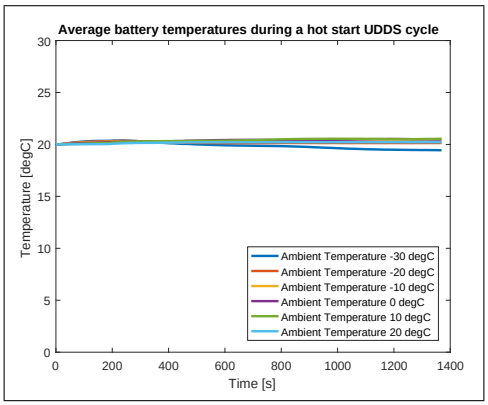

Figure 32: Average battery temperature during a HS UDDS cycle.

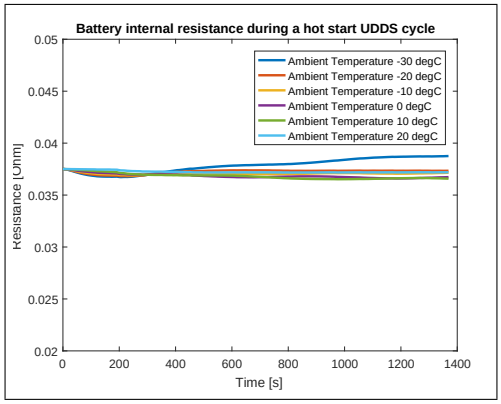

Figure 33: Battery internal resistance during a HS UDDS cycle for one module.

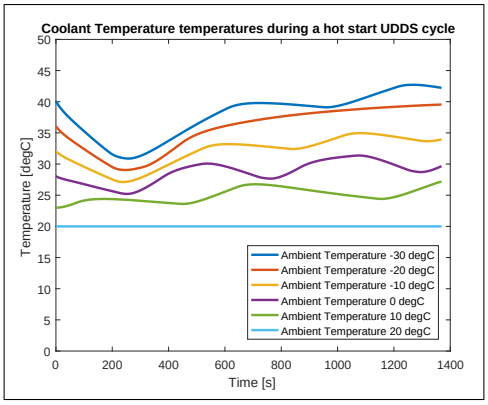

Figure 34: Coolant temperature during a HS UDDS cycle.

G Hot Start HWY Drive Cycle for Results the Baseline Model

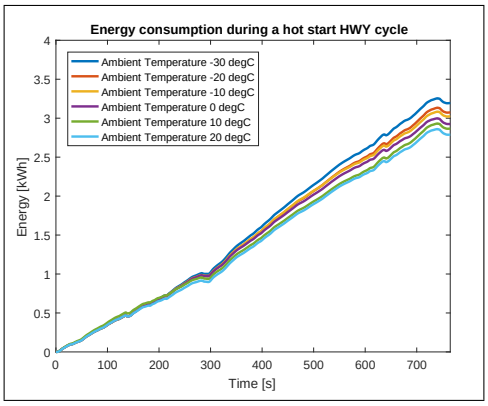

Figure 35: Simulated cumulative energy consumption in kWh during a HS HWY cycle.

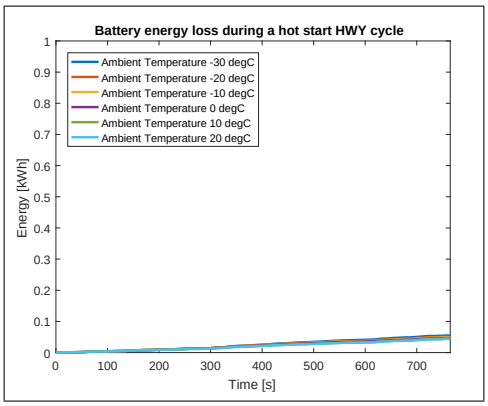

Figure 36: Simulated cumulative energy loss in kWh during a HS HWY cycle.

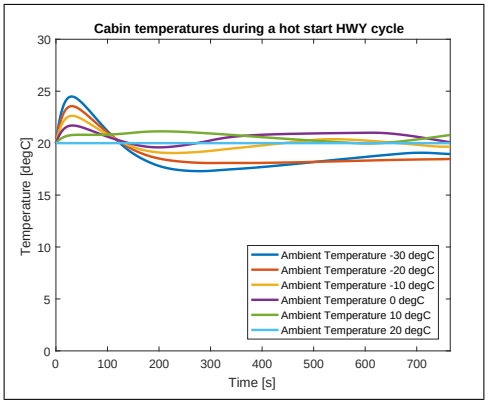

Figure 37: Cabin temperature during a HS HWY cycle.

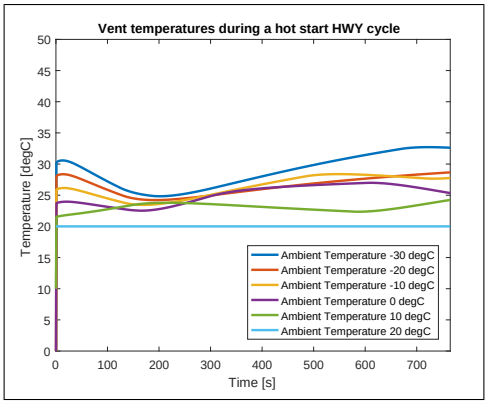

Figure 38: Vent temperature during a HS HWY cycle.

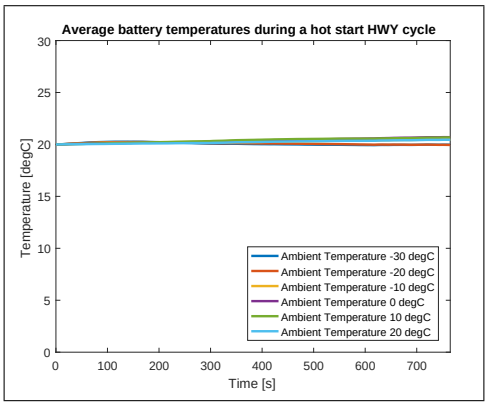

Figure 39: Average battery temperature during a HS HWY cycle.

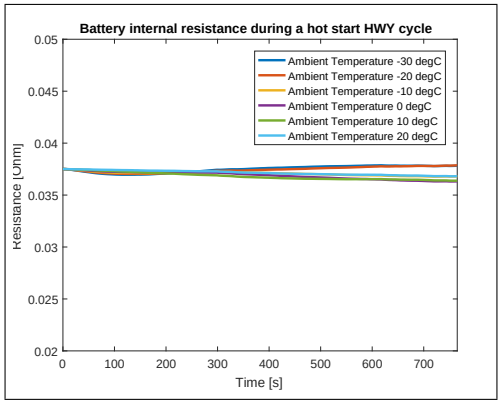

Figure 40: Battery internal resistance during a HS HWY cycle for one module.

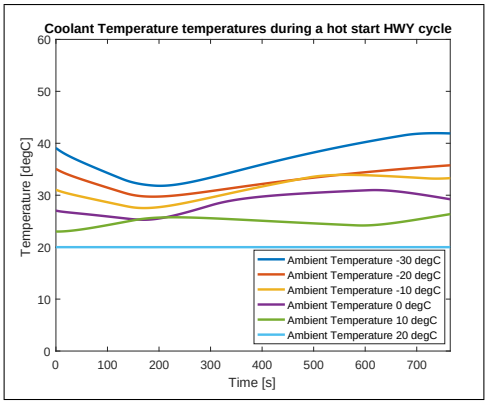

Figure 41: Coolant temperature during a HS HWY cycle.

H Data Used for Optimal Mass Calculation

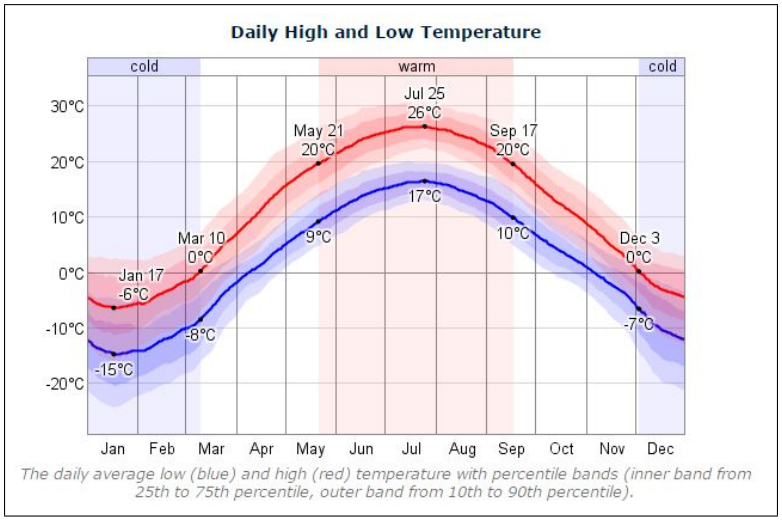

Figure 42: Average daily high and low temperatures for Ottawa, Canada [49].

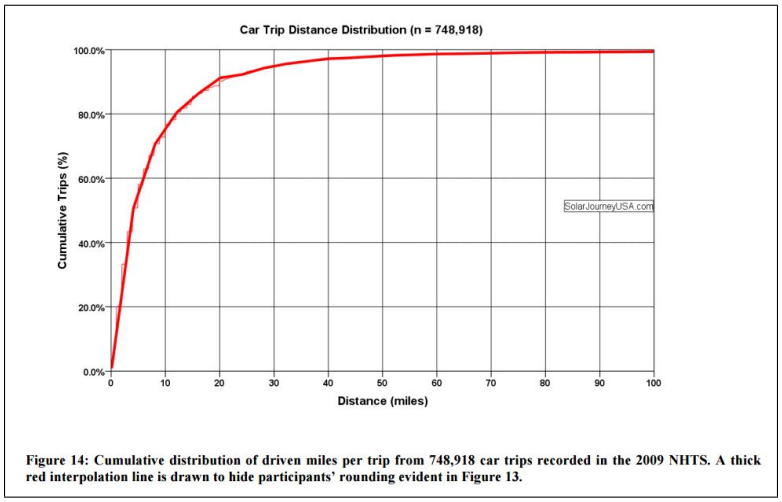

Figure 43: Average trip length [48].

References

[1] Windows to the Universe, "Solar Energy in Earth's Atmosphere." [Online]. Available: http://www.windows2universe.org/earth/Atmosphere/earth_atmosph_radiation_budget.html

[2] Intergovernmental Panel on Clima Change, *Climate Change 2013*, 2013.

[3] Ontario Government, "Climate Change Action Plan." [Online]. Available: https://www.ontario.ca/page/climate-change-action-plan#section-3

[4] U.S. Evironmental Protection Agency, "Global Greenhouse Gas Emissions Data." [Online]. Available: https://www.epa.gov/ghgemissions/global-greenhouse-gas-emissions-data

[5] K. Umezu and H. Noyama, "Air-Conditioning system For Electric Vehicles (i-MiEV)," *SAE Automotive Refrigerant & System Efficiency Symposium 2010*, pp. 1–20, 2010. [Online]. Available: http://www.sae.org/events/aars/presentations/2010/W2.pdf

[6] H. Lohse-Busch, M. Duoba, E. Rask, and M. Meyer, "Advanced Powertrain Research Facility AVTA Nissan Leaf testing and analysis," Argonne National Laboratory, Tech. Rep., 2012.

[7] M. Allen, "Real-world range ramifications: heating and air conditioning," 2014. [Online]. Available: http://www.fleetcarma.com/electric-vehicle-heating-chevrolet-volt-nissan-leaf/

[8] A. Doyle, T. Muneer, and I. Smith, "A review of the thermal performance of Electric Vehicles," pp. 1–5, 1992.

[9] V. Bradshaw, *The Building Environment: Active and Passive Control Systems*, 3rd ed. Hoboken: John Wiley & Sons, 2006. [Online]. Available: http://courses.washington.edu/me333afe/Comfort_Health.pdf

[10] M. Wawzyniak, M. Jung, and J. Haug, "Holistic Thermal Management of Electric Vehicles."

[11] L. Chaney, M. A. Jeffers, and J. P. Rugh, "Climate Contorl Load Reduction Strategies for Electric Drive Vehicles in Cold Weather Motivation Cabin Heating Can Significantly Reduce EV Range," no. April, pp. 21–23, 2015.

[12] J. R. M. Delos Reyes, R. V. Parsons, and R. Hoemsen, "Winter Happens: The Effect of Ambient Temperature on the Travel Range of Electric Vehicles," *IEEE Transactions on Vehicular Technology*, vol. 65, no. 6, pp. 4016–4022, 2016.

[13] Repair Pal, "Heating and Air Conditioning." [Online]. Available: http://repairpal.com/heating-ac

[14] R. Musat and E. Helerea, "Characteristics of the PTC heater used in automotive HVAC systems," *IFIP Advances in Information and Communication Technology*, vol. 314, pp. 461–468, 2010.

[15] M. Shams-Zahraei, A. Z. Kouzani, S. Kutter, and B. Bäker, "Integrated thermal and energy management of plug-in hybrid electric vehicles," *Journal of Power Sources*, vol. 216, pp. 237–248, 2012.

[16] Q. Peng and Q. Du, "Progress in heat pump air conditioning systems for electric vehicles-A review," *Energies*, vol. 9, no. 4, 2016.

[17] B. Randall, "Tesla - Blowing Hot and Cold," 2006. [Online]. Available: https://www.tesla.com/blog/blowing-hot-and-cold

[18] Z. Shi, S. Vadera, A. Aamodt, and D. Leake, *IFIP Advances in Information and Communication Technology: Preface*, 2010, vol. 340 AICT.

[19] Mitsubishi, "PTC Heater for Electric Vehicles and Plug-in Hybrid Vehicles Using Water Heat Carrier," Tech. Rep. 4, 2010.

[20] T. Bäuml, D. Dvorak, A. Frohner, and D. Simic, "Simulation and Measurement of an Energy Efficient Infrared Radiation Heating of a Full Electric Vehicle," 2014.

[21] NREL, "NREL Reveals Links Among Climate Control, Battery Life, and Electric Vehicle Range," 2012.

[22] "49 CFR 571.103 - Standard No. 103; Windshield defrosting and defogging systems." [Online]. Available: https://www.law.cornell.edu/cfr/text/49/571.103

[23] J. Cao and A. Emadi, "A New Battery/UltraCapacitor Hybrid Energy Storage System for Electric, Hybrid, and Plug-In Hybrid Electric Vehicles," *Power Electronics, IEEE Transactions on*, vol. 27, no. 1, 2012. [Online]. Available: http://ieeexplore.ieee.org/xpl/articleDetails.jsp?arnumber=5764539

[24] M. Ehsani, Y. Gao, and A. Emadi, *Modern Electric, Hybrid Electric, and Fuel Cell Vehicles*, 2nd ed. CRC Press, 2010.

[25] A. Emadi, *Advanced Electric Drive Vehicles*. CRC Press, 2015. [Online]. Available: https://www.crcpress.com/Advanced-Electric-Drive-Vehicles/Emadi/p/book/9781466597693

[26] A. Sharma, V. V. Tyagi, C. R. Chen, and D. Buddhi, "Review on thermal energy storage with phase change materials and applications," *Renewable and Sustainable Energy Reviews*, vol. 13, no. 2, pp. 318–345, 2009.

[27] A. Ugurlu and C. Gokcol, "A Review on Thermal Energy Storage Systems With Phase Change Materials in Vehicles," *Electronic Journal of Vocational Colleges*, pp. 1–14, 2012.

[28] F. A. Wyczalek, "Heating and Cooling Battery Electric Vehicles - The Final Barrier," *IEEE Aerospace and Electronic Systems Magazine*, vol. 8, no. 11, pp. 9–14, 1993.

[29] M. Wang, E. Wolfe, T. Craig, T. J. Laclair, O. Abdelaziz, and Z. Gao, "Design and Testing of a Thermal Storage System for Electric Vehicle Cabin Heating," 2016. [Online]. Available: http://papers.sae.org/2016-01-0248/\nhttps://www.newswire.com/news/pcm-based-system-heats-electric-vehicle-without-draining-4683778-11304520

[30] L. Broglia, G. Autefage, and M. Ponchant, "Impact of passenger thermal comfort and electric devices temperature on range: A system simulation approach," *World Electric Vehicle Journal*, vol. 5, no. 4, pp. 1082–1089, 2012.

[31] M. A. Fayazbakhsh and M. Bahrami, "Comprehensive Modeling of Vehicle Air Conditioning Loads Using Heat Balance Method," *SAE Transactions*, no. x, 2013. [Online]. Available: http://www.sfu.ca/ mbahrami/pdf/2013/Comprehensive Modeling of Vehicle Air Conditioning Loads Using Heat Balance Method.pdf\nhttp://www.sae.org/technical/papers/2013-01-1507

[32] K. R. Kambly and T. H. Bradley, "Estimating the HVAC energy consumption of plug-in electric vehicles," *Journal of Power Sources*, vol. 259, pp. 117–124, 2014. [Online]. Available: http://dx.doi.org/10.1016/j.jpowsour.2014.02.033

[33] R. Valentina, A. Viehl, O. Bringmann, and W. Rosenstiel, "HVAC system modeling for range prediction of electric vehicles," *IEEE Intelligent Vehicles Symposium, Proceedings*, no. Iv, pp. 1145–1150, 2014.

[34] J. Neubauer and E. Wood, "Thru-life impacts of driver aggression, climate, cabin thermal management, and battery thermal management on battery electric vehicle utility," *Journal of Power Sources*, vol. 259, pp. 262–275, 2014. [Online]. Available: http://dx.doi.org/10.1016/j.jpowsour.2014.02.083

[35] "Climate Control and AUTO Mode Guide - My Nissan Leaf Forum," 2013. [Online]. Available: http://www.mynissanleaf.com/viewtopic.php?t=7743

[36] Qnovov, "69. Inside the Battery of a Nissan Leaf," 2015. [Online]. Available: http://qnovo.com/inside-the-battery-of-a-nissan-leaf/

[37] U.S. Department of Energy, "2011 Nissan Leaf." [Online]. Available: http://media3.ev-tv.me/DOEleaftest.pdf

[38] J. G. Hayes and K. Davis, "Simplified electric vehicle powertrain model for range and energy consumption based on EPA coast-down parameters and test validation by Argonne National Lab data on the Nissan Leaf," *2014 IEEE Transportation Electrification Conference and Expo (ITEC)*, no. June, pp. 1–6, 2014. [Online]. Available: http://ieeexplore.ieee.org/lpdocs/epic03/wrapper.htm?arnumber=6861831

[39] D. Sherman, "2012 Nissan Leaf SL." [Online]. Available: http://www.caranddriver.com/features/drag-queens-aerodynamics-compared-comparison-test-fifth-place-nissan-leaf-page-2

[40] Nissan, "Nissan Leaf." [Online]. Available: https://www.nissanusa.com/electric-cars/leaf/versions-specs/

[41] Wheel-size, "Nissan Leaf 2012 Alloy wheel fitment guide." [Online]. Available: https://www.wheel-size.com/size/nissan/leaf/2012/

[42] DieselNet, "Emission Test Cycles FTP-72 (UDDS)." [Online]. Available: https://www.dieselnet.com/standards/cycles/ftp72.php

[43] DieselNet, "Emission Test Cycles EPA Highway Fuel Economy Test Cycle (HWFET)." [Online]. Available: https://www.dieselnet.com/standards/cycles/hwfet.php

[44] A. D. Brooker, J. Ward, and L. Wang, "Lightweighting Impacts on Fuel Economy, Cost, and Component Losses," *SAE World Congress & Exhibition, SAE paper 2013-01-0381*, vol. 2013-01-03, p. 10, 2013. [Online]. Available: http://www.sae.org/technical/papers/2013-01-0381

[45] A. Casadei and R. Broda, "Impact of Vehicle Weight Reduction on Fuel Economy for Various Vehicle Architectures." [Online]. Available: http://www.drivealuminum.org/wp-content/uploads/2016/07/Ricardo_Impact-of-Vehicle-Weight-Reduction-on-Fuel-Economy-for-Various-Vehicle-Architectures.pdf

[46] Wikipedia, "Nissan Leaf." [Online]. Available: https://en.wikipedia.org/wiki/Nissan_Leaf

[47] P. N. Drive, "A Guide to EV Charging." [Online]. Available: http://www.plugndrive.ca/guide-ev-charging

[48] R. Van Haaren, "Assessment of electric cars ' range requirements and usage patterns based on driving behavior recorded in the National Household Travel Survey of 2009," *Earth and Environmental Engineering Department, Columbia University, Fu Foundation School of Engineering and Applied Science, New York*, vol. 1, no. 917, p. 56, 2012.

[49] WeatherSpark, "Average Weather For Ottawa, Ontario, Canada." [Online]. Available: https://weatherspark.com/averages/28316/Ottawa-Ontario-Canada